Novel observations of East Asian Summer Monsoon evolution during Glacial Termination II from Lake Suigetsu, Japan

Rex, Charlie L.[1,2], Staff, Richard A.[1], Toney, Jaime L.[2], Pearson, Emma J.[3], Francke, Alexander[4,5], Saito-Kato, Megumi[6], Nakagawa, Takeshi[6]*

** Corresponding author (c.rex.1@research.gla.ac.uk)*

1. Scottish Universities Environmental Research Centre (SUERC), University of Glasgow, Scottish Enterprise Technology Park, Rankine Avenue, East Kilbride, G75 0QF, United Kingdom
2. School of Geographical and Earth Sciences, University of Glasgow, Glasgow, G12 8QQ, United Kingdom
3. School of Geography, Politics and Sociology, Newcastle University, Newcastle upon Tyne, NE1 7RU, United Kingdom
4. Discipline of Earth Science, School of Physics, Chemistry and Earth Sciences, University of Adelaide, 5005 Adelaide, South Australia, Australia
5. Discipline of Archaeology, College of Humanities, Arts and Social Sciences, Flinders University, 5042 Adelaide, South Australia, Australia
6. Department of Geology and Paleontology, National Museum of Nature and Science, 4-1-1 Amakubo, Tsukuba-shi, Ibaraki Prefecture, 3050005, Japan
7. Research Centre for Palaeoclimatology, Ritsumeikan University, 1-chōme-1 Nojihigashi, Kusatsu, Shiga Prefecture, 525-0058, Japan

This is a non-peer reviewed preprint submitted to EarthArXiv.

Abstract

Glacial terminations offer a unique opportunity to examine how the East Asian Summer Monsoon (EASM) responds to rapid increases in global temperature and accompanying abrupt climatic reorganisation. Reconstructions from contrasting glacial terminations with differently evolving boundary conditions are of particular value to our understanding of deglacial EASM behaviours, e.g., Termination I (from MIS 2 to MIS 1) and Termination II (from MIS 6 to MIS 5e). However, records of EASM evolution across Termination II are substantially fewer in number than Termination I, as well as exhibiting a significant bias towards continental speleothem archives. Japan is a critically understudied, but demonstrably sensitive area of the EASM region and, during other periods, records from Japan often display unique trends not captured by continental records. Here we present a new EASM record derived from the Lake Suigetsu sediment cores, central Japan, based on compound-specific hydrogen isotope analysis of C_{30} n-alkanoic acids ($\delta^2H_{C30acid}$), which constitutes the first stable isotope-based EASM record from the Japanese archipelago across Termination II. We also present lipid biomarker (n-alkane and n-alkanoic acid) concentrations and indices, which we use to reconstruct early lake formation. The catchment transitioned from a dynamic fluvial environment to a lacustrine one between 131.0 and 129.8 ka BP. The EASM strengthened from 132.5 to 130.0 ka BP (earlier than in continental China), before weakening toward 125.2 ka BP, with some evidence for submillennial-scale variability during this weakening phase; a pattern common to sites across the EASM region which are closer to the northernmost position of the monsoon front. Whilst our record displays some similar characteristics to EASM reconstructions from mainland China, our observations support the assertion that EASM behaviours during Termination II were spatially heterogeneous. Additionally, comparison of our Termination II $\delta^2H_{C30acid}$ record to a record of $\delta^2H_{C30acid}$ from Lake Suigetsu during

Termination I suggests that EASM evolution during the last and penultimate deglaciations were distinct due to differently evolving climatic conditions (including the extreme decoupling of polar temperatures during Termination II). We propose that the spatial heterogeneities in EASM strength during Termination II were a result of competing influences from the Northern and Southern Hemispheres, with Japan more closely linked to the latter compared to mainland China due to its maritime location.

Keywords

Quaternary; Paleoclimatology; Paleolimnology; Eastern Asia; Continental Biomarkers; Organic Geochemistry; Stable Isotopes; Japan; Glacial Termination; East Asian Summer Monsoon

Highlights

- The first stable isotope-based reconstruction of EASM behaviour from Japan during TII.
- The EASM in Japan strengthened to 130.0 ka BP before weakening to 125.2 ka BP.
- Evidence for submillennial-scale variability in EASM strength.
- EASM strengthening across TII occurred earlier in Japan than mainland China.
- Evidence for competing northern and southern hemisphere influences on the EASM.

1.0 Introduction

The East Asian Summer Monsoon (EASM) system exerts significant influence on the water resource distribution and climatic hazards of East Asia, making this densely populated region vulnerable to the spatial and temporal redistribution of EASM precipitation due to anthropogenic climate change (Chen et al., 2019; Park et al., 2019). By characterising EASM behaviours across glacial terminations, it is possible to examine how the system operated under, and during the rapid transition between, previous extremes of global temperature (He et al., 2017; Duan et al., 2019). Critically, glacial terminations exemplify a greater amplitude of climatic change than is currently covered by contemporary observations of the EASM system. Furthermore, whilst there are differences between glacial terminations and present-day anthropogenic warming, the study of the former provides improved knowledge of how EASM evolution coevolves with abrupt global climate system reorganisation (He et al., 2017). In particular, the sub-structure of EASM behaviour across deglacial intervals can shed light on the relationship between the EASM and coupled atmosphere-ocean circulations, which can be significant drivers of EASM strength on centennial-to-millennial timescales (Wang et al., 2008; Zhang et al., 2019).

EASM evolution across the last glacial termination (TI; the transition from MIS 2 to MIS 1) is relatively well-studied (albeit less comprehensively than other regional climate systems, such as the North Atlantic) with reasonable coverage provided by a growing network of high-quality palaeoclimate records (e.g., Wang et al., 2001; Wang et al., 2010; Zhang et al., 2018). Contrastingly, records of EASM behaviour across the penultimate glacial termination (TII; the transition from MIS 6 to MIS 5e) are substantially fewer in number (He et al., 2017; Duan et al., 2019), likely due to a combination of poor archive preservation across this older interval and a preference for studying time periods where high-resolution chronological control is more easily obtained (i.e., within the limit of radiocarbon dating). However, our collective knowledge regarding how the EASM responds to rising temperatures is substantially enriched by reconstructions from across a range of boundary conditions. The sequences of deglacial climate change which occurred during TI and TII were characteristically different (Figure 1;

Gorbarenko et al., 2019), meaning that there is inherent value in targeting EASM reconstructions from TII to complement the growing compilation of records covering TI (He et al., 2017). Both TI and TII exhibited asymmetrical hemispheric warming (whereby the southern hemisphere warmed prior to the Northern Hemisphere) (Figure 1; Broecker and Henderson, 1998; Masson-Delmotte et al., 2010); however, whilst there is convincing evidence for the submillennial-scale sub-structure of temperature evolution during TI (e.g., the North Atlantic Bølling–Allerød/Younger Dryas, or the Antarctic Cold Reversal (Rasmussen et al., 2014; WAIS Divide Project Members, 2013), the evidence for similar variability during TII is equivocal (Figure 1; Cheng et al., 2019; Duan et al., 2019). Furthermore, there is evidence to suggest that TII was associated with more rapid sea surface temperature increases, sea level rise and ice sheet collapse relative to TI (Caley et al., 2013), making it a useful interval to study in order to better understand how the EASM might evolve under future climate scenarios.

Current EASM reconstructions from TII are heavily weighted towards $\delta^{18}O_{speleothem}$ records from China, which provide evidence for a weak EASM in the latter stages of MIS 6 (posited as temporally equivalent to Heinrich Event 11) (Yuan et al., 2004; Cheng et al., 2006; Duan et al., 2019), followed by rapid EASM strengthening across a sub-200-year interval at ~129 ka BP (Kelly et al., 2006; Duan et al., 2019) and a relatively strong EASM during the early stages of MIS 5e (Li et al., 2014), persisting to ~121 ka BP (Kelly et al., 2006). The rate of EASM strengthening at ~129 ka BP has been proposed as evidence for threshold behaviour (Yuan et al., 2004), with this shift coinciding with increasing Northern Hemisphere temperatures and Northern Hemisphere ice sheet collapse (Jiang et al., 2005; Oppo and Sun, 2005; Cheng et al., 2006) but lagging behind Northern Hemisphere summer insolation, Antarctic temperature, atmospheric CO_2 concentration and sea level rise (Yuan et al., 2004; Wang et al., 2008; Xue et al., 2019).

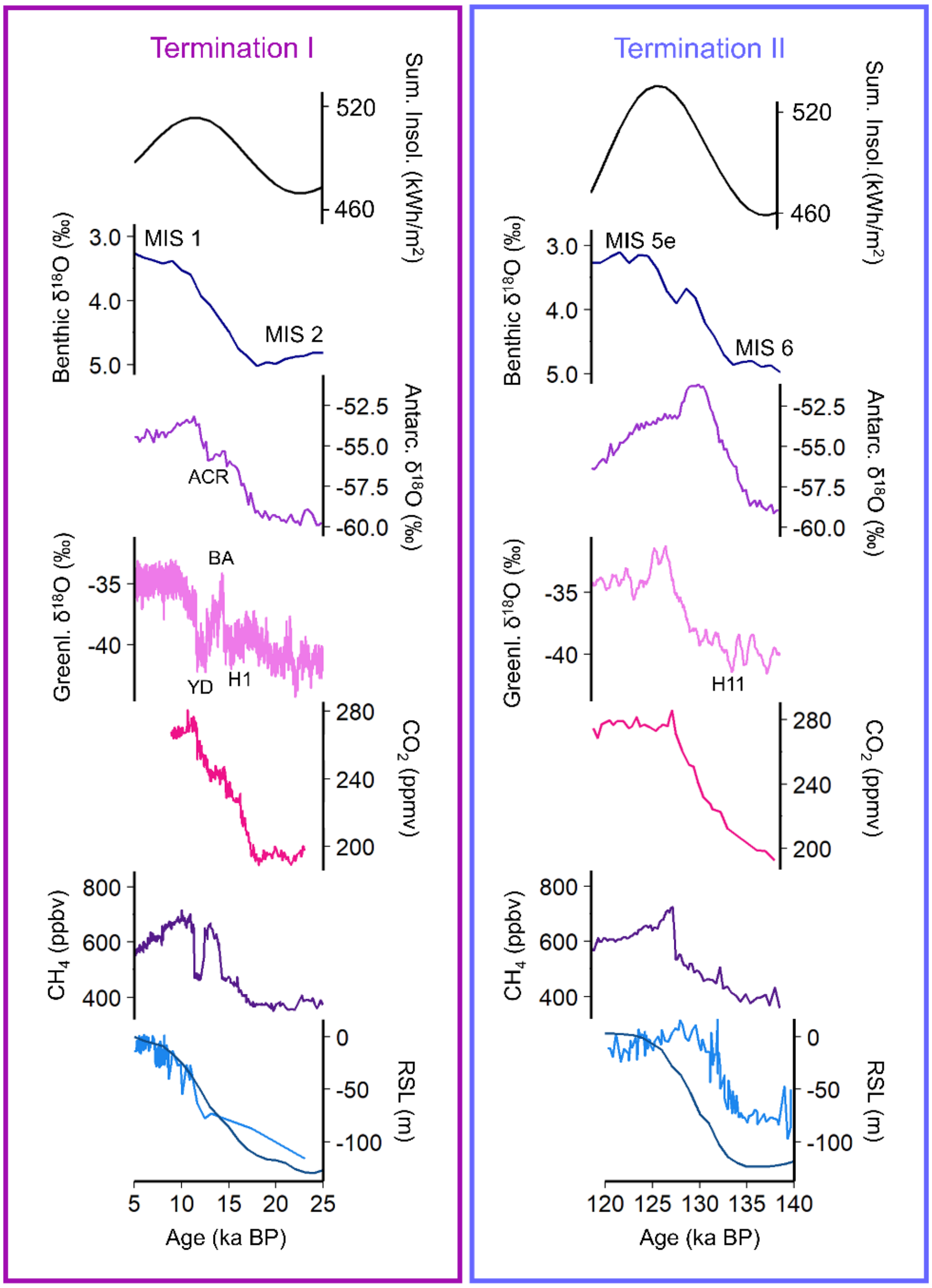

Figure 1 – The differences between the climatic sequences of TI and TII (adapted from Barker and Knorr, 2021). The reconstructions shown, from top to bottom, are: June Insolation at 30°N (Laskar et al., 2004); the Global Benthic $\delta^{18}O$ stack (Lisiecki and Raymo, 2005); Dome Fuji Antarctic $\delta^{18}O_{ice}$ (Kawamura et al., 2007); GRIP (TI; Johnsen et al., 1997; Rasmussen et al., 2014) and Synthetic (TII; Barker et al., 2011) Greenland $\delta^{18}O_{ice}$; WAIS Divide (TI; Marcott et al., 2014) and Dome Fuji (TII; Kawamura et al., 2007) atmospheric CO_2 concentration; EPICA Dome C Atmospheric CH_4 concentration (Loulergue et al., 2008); and Relative Sea Level (RSL; Grant et al., 2014 (light blue); Spratt and Lisiecki, 2016 (dark blue)). Abbreviations: MIS = Marine Isotope Stage, ACR = Antarctic Cold Reversal, YD = Younger Dryas, BA = Bølling–Allerød, H1 = Heinrich Event 1, H11 = Heinrich Event 11.

However, the submillennial-scale structure of EASM strength variations during this period is highly debated (much like the temperature profiles of the same interval). Some records (e.g., Hulu Cave) show smooth EASM strengthening with no evidence for submillennial-scale fluctuations (Cheng et al., 2006), however others show varying degrees of sub-structure within the overall EASM strengthening trend. At Dongge Cave and Sanbao Cave, EASM strength exhibited a post-transition “slowdown” and increased more slowly after a sudden upturn at 129 ka BP (Jiang et al., 2005; Kelly et al., 2006). At Xinglong Cave, there was a notable “pause” in EASM strengthening (Duan et al., 2019), attributed to muted “Younger Dryas”-type stadial conditions in the North Atlantic. It was proposed that this interval was associated with a smaller amplitude of cooling than the TI Younger Dryas due to a severely supressed Atlantic Meridional Overturning Circulation (AMOC) during TII which was not as significantly perturbed by meltwater pulses. At Shangxiaofeng Cave, a full inversion of EASM strength was detected, likely in response to short lived (~400 year) stadial conditions, again attributed to “Younger Dryas”-type conditions (Xue et al., 2019). These conflicting observations suggest that EASM evolution across TII exhibits greater spatial heterogeneity than across TI (Xue et al., 2019).

To tackle the uncertainty surrounding EASM evolution across TII and the substantial bias towards continental $\delta^{18}O_{speleothem}$ records, we present a new compound specific stable isotope-based ($\delta^{2}H_{C30acid}$) EASM record derived from the Lake Suigetsu sediment cores, central Japan. Japan is situated in a critically understudied, yet demonstrably sensitive, area of the East Asian Monsoon region, being situated beneath the seasonally migrating monsoon front (north of it during winter and south of it during summer) and receives a significant proportion of its rainfall annually from the EASM (Nakagawa et al., 2006). Reconstructions of climate (including EASM behaviour) across TI from Japan have shown the potential of this area for deconvolving complexities in the responses of temperature and precipitation to deglaciation (Hayashi et al., 2010; Liepe et al., 2015; Nakagawa et al., 2021). Our new record constitutes the first terrestrial stable isotope-based EASM record from Japan across TII, providing novel insights into EASM evolution across this interval from a region that is sensitive to EASM fluctuations. The results of this study are complemented by equivalent analysis from TI (Rex et al., 2023a, preprint), facilitating the direct comparison of EASM evolution at Lake Suigetsu across the penultimate and last glacial terminations.

Our approach constitutes two complementary techniques employing lipid biomarkers preserved within the Lake Suigetsu sediment cores: determination of the compound-specific hydrogen isotope composition of n-alkanoic acids (δ^2H_{acid}) from terrestrial leaf waxes to reconstruct regional EASM behaviour; and quantification of terrestrial (leaf wax-derived; long-chained) and aquatic (algae-derived; short-chained) n-alkane and n-alkanoic acid concentrations to account for local (catchment) scale changes. The hydrogen isotope composition of terrestrial leaf waxes preserved within sediments is becoming increasingly utilised for palaeohydrological reconstructions in light of its close relationship to the hydrogen isotope composition of past precipitation ($\delta^2H_{precipitation}$) which would have provided the source water for plant growth (Sachse et al., 2012; Holtvoeth et al., 2019). As such, δ^2H_{acid} can act as a tracer for shifts in atmospheric circulation and vapour transport (Tierney et al., 2008) which is stable on geological timescales (Sachse et al., 2006). Within the context of the Lake Suigetsu catchment, $\delta^2H_{precipitation}$ during the growth season is dominantly controlled by EASM behaviour (Rex et al., 2023b, preprint) and hence δ^2H_{acid} has demonstrable links to the regional EASM system, facilitating reconstructions of past EASM variability. Owing to the significant catchment evolution which occurred at Lake Suigetsu during TII, we also make use of terrestrial (long-chained) and aquatic (short-chained) homologue concentrations alongside existing diatom species counts, TOC/TN and $\delta^{13}C_{org}$ analyses to examine local environmental change more closely across this hitherto weakly constrained interval.

2.0 Study site

Lake Suigetsu is a ~34 m deep tectonic lake located adjacent to the Sea of Japan in Fukui Prefecture, Honshu Island, central Japan (35˚35'08" N, 135˚52'57" E) (Figure 2; Nakagawa et al., 2021). The lake is relatively small, with a surface area of approximately 4.2 km^2 (Shigematsu et al., 1961), occupying ~50 % of its total direct catchment area. Suigetsu is one of the "Five Lakes of Mikata", a lake system which, in the modern day, forms a series of artificially interconnected water bodies linking the Hasu River to the south and Wakasa Bay to the north (Figure 2; Shigematsu et al., 1961; Nakagawa et al., 2021). The climate of the catchment is typical of the Sea of Japan coast of Honshu Island; i.e., temperate and monsoonal. Between May and July, the climate of the region is dominated by the moisture-rich south-easterly winds of the EASM (Nakagawa et al., 2006; Chowdary et al., 2019). During these months the area receives large quantities of precipitation during the northward propagation of the EASM front, which usually reaches the catchment in June and delivers water derived from the Pacific Ocean (Nakagawa et al., 2006; Schlolaut et al., 2014). The region also receives a very large quantity of East Asian Winter Monsoon (EAWM) precipitation (mixed snowfall and rainfall) between December and February each year (Nakagawa et al., 2012). The strong seasonality of precipitation delivered to the catchment means that both East Asian Monsoon modes are detectable in isolation when sampling is undertaken on seasonal timescales (Rex et al., 2023b, preprint).

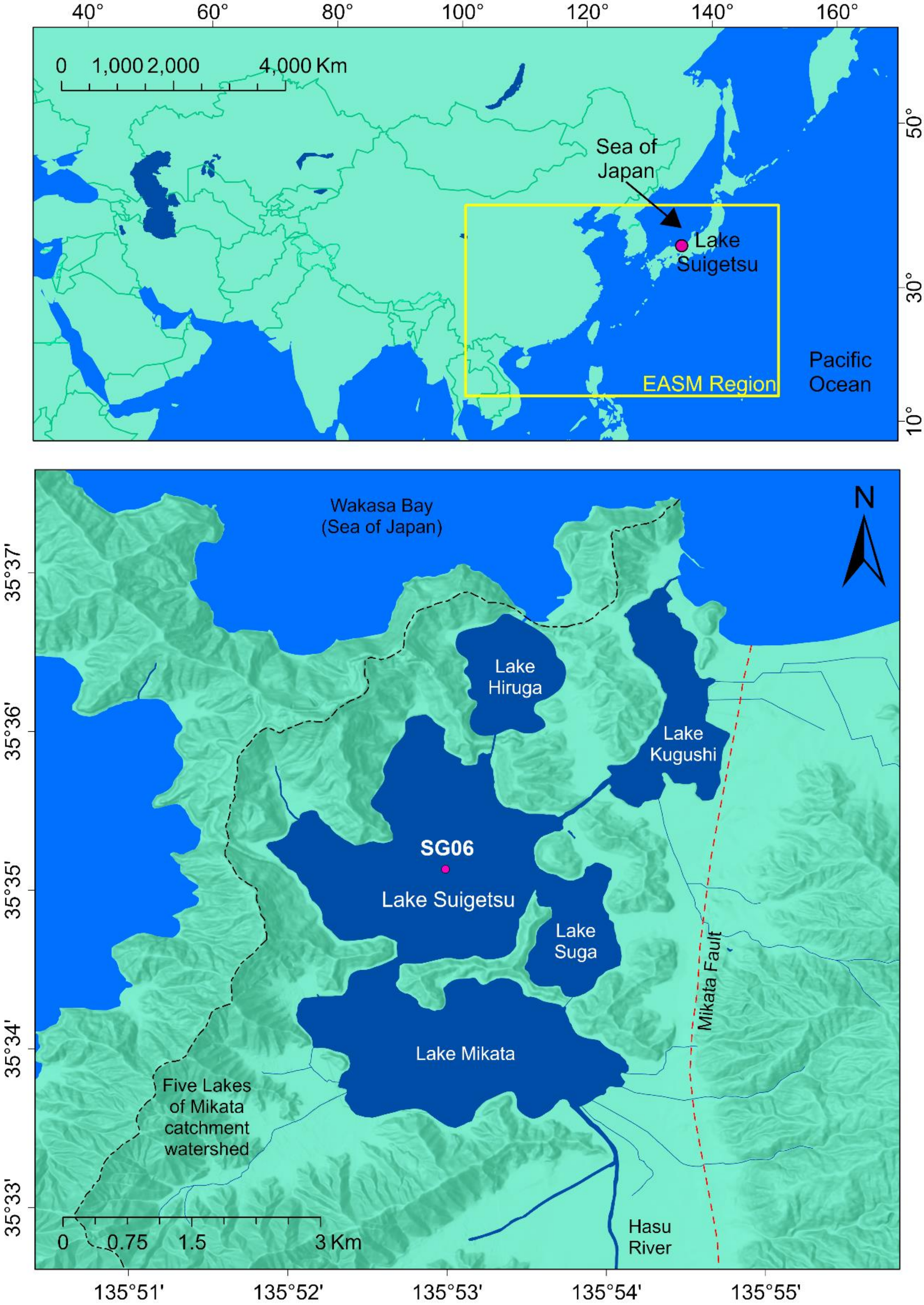

Figure 2 – The location of Lake Suigetsu and the Five Lakes of Mikata. The upper panel shows the position of Lake Suigetsu within the EASM region. The lower panel shows the modern-day lake configuration relative to the Mikata Fault, the Hasu River and the Sea of Japan. The catchment watershed is also indicated. Basemap is a custom Light Grey Canvas with World Hillshade from Esri (2023a; 2023b) (scale 1:66,623,747 (upper panel), 1:43,517 (lower panel)).

A series of deep coring campaigns across the past 30 years have excavated materials from below the lake to generate a world-leading palaeoenvironmental archive which spans >98 m of composite depth (from the present day to in excess of 200 ka BP; Nakagawa et al., 2012; McLean et al., 2018). As such, the Lake Suigetsu sediment cores are a rare example of a well preserved, continuous sediment record which extends to the penultimate glacial period (Nakagawa et al., 2012; Rex et al., 2022). Indeed, the upper ~45 m form the longest continuously varved record from the Quaternary (Schlolaut et al., 2012; Schlolaut et al., 2018). The composition and sedimentology of the cores varies through time, driven by the evolution of the Five Lakes of Mikata system from its origin to the present-day configuration. This process was principally driven by subsidence of the western side of the Mikata Fault (which lies <2 km to the east of the lakes) creating accommodation space for the lakes and causing lake deepening with time (Suzuki et al., 2016). The area was perhaps at its most dynamic during TII; the area shifted between fluvial and shallow water environments during MIS 6 (Nakagawa et al., 2012; Rex et al., 2022), before evolving into a lake system. As such, the oldest sediments from Lake Suigetsu are principally a mixture of peats and clays (the latter sometimes finely laminated; Francke et al., in prep). By MIS 5e, the area was an established lake system, which became saline during the Eemian global sea level highstand due to saltwater incursions from the Sea of Japan, as evidenced by the presence of brackish-tolerant diatom species (Saito-Kato et al., in prep; Nakagawa et al., 2021). Sediments from this interval are finely laminated and it is inferred from this that the water column was sufficiently deep to prevent turbation by surface winds (and possibly had anoxic bottom waters, which hindered bioturbation).

3.0 Materials and methods

3.1 Core materials

Materials for this study were obtained from the 73.2 m Lake Suigetsu “SG06” core (Figure 2), extracted from the centre of Lake Suigetsu as overlapping core sections from four parallel boreholes (Nakagawa et al., 2012). Alignment of the core sections was conducted using visible marker horizons to create a composite master core. Chronological control for the younger part of the core (upper ~40 m of composite depth; ~50 ka BP to the present day) is provided by >800 radiocarbon dates, thin section microscopic varve counting and geochemically identified volcanic tephra layers (Bronk Ramsey et al., 2020; Staff et al., in prep). However, the older part of the core (from ~40 – 73 m composite depth) is beyond the limit of the radiocarbon dating technique and contains only discontinuous varved sections (to ~45 m composite depth), and hence alternative chronological techniques must be used to produce an extension of this age depth model. The most recent iteration of this extension (Francke et al., in prep) aligns the relative abundance of *Cryptomeria* pollen in SG06 to the same quantity in MD2421-01, a marine core from offshore Japan in the Pacific Ocean (Oba et al., 2006). This process was supplemented by cross-archive alignment of the Aso-4 tephra (86.4 ± 1.1 Ar-Ar ka BP) as an absolute chronological tie point (Albert *et al*., 2019). The oxygen isotope stratigraphy of MD2421-01 was updated as part of this procedure by alignment to the regional benthic isotope stack for the Pacific (Lisiecki and Stern, 2016). The ages presented in this study are given in thousand years before 1950 CE (“ka BP”) because the complete (i.e., combined radiocarbon and non-radiocarbon) Suigetsu core chronology has a datum at 1950 CE. This iteration of the chronology indicates that the oldest sediments within the SG06 core were deposited ~146 ka BP (i.e., MIS 6). The age-depth model of MD2421-01 is aligned to other global palaeoclimate archives (e.g., the Greenland ice cores and Chinese speleothems) via the Pacific regional benthic isotope stack (Lisiecki and Stern, 2016).

Sediment was extracted from longitudinally cut core sections as ~58-year (n = 56) or ~112-year (n = 4) contiguous (continuous adjacent) subsamples spanning 125.23 ± 2.26 to 132.62 ± 2.20 ka BP (6389.5 to 6908.2 cm composite depth (ver. 06 April 2020)). This interval was selected to bracket the period of most rapid EASM change during TII (~128 ka BP) as evidenced by the Chinese speleothems (e.g., Jiang et al., 2005; Cheng et al., 2006), as well as extremes in preliminary, low-resolution pollen-derived temperature from the Suigetsu cores. Core expansion during storage was accounted for by linear interpolation (Rex et al., 2023a, preprint). Care was taken to remove the outer ~3 mm of sediment before subsampling in order to eliminate the possibility of cross-contamination by modern organic compounds from handling during core extraction (Rex et al., 2023a, preprint). In the same vein, instruments and surfaces were cleaned with ethanol prior to use. Sample wet weights ranged from 5.4 – 13.6 g. To prevent skewing of the results to large instantaneous events, event layers (such as tephra and flood materials) were removed where possible prior to subsampling. It is important to note that because the target sediments were varied in type and colour, some event layers may have been overlooked. However, this cautious approach is preferable to a more stringent one, which could result in accidental omission of non-event material. Plant macrofossils were also removed following the same logic (i.e., that a large amount of material from a single organic fossil could skew the analytical results of that sample). Whilst the sediments extracted as part of this process were well preserved, it is possible that bioturbation and discontinuous deposition was undetected on account of the lack of consistent sedimentary substructure (i.e., varving).

3.2 Sample preparation

Samples were prepared for analysis (in batches of 10 samples, each with a procedural blank) at the University of Glasgow following an amended version of the preparation methodology presented in Rex et al. (2023a, preprint). A Total Neutral Fraction (TNF) and a Total Acid Fraction (TAF) were extracted from each freeze-dried sediment sample by an Accelerated Solvent Extractor using dichloromethane and methanol (9:1, v:v) (to yield the total lipid extract), followed by solid phase extraction through a LC-NH_2 silica gel column. A dichloromethane:propan-2-ol solution (1:1, v:v) and 4 % acetic acid in diethyl ether were used to elute the TNF and TAF, respectively. The TNF was further separated through a silica gel column; the first neutral fraction (N1, containing aliphatic hydrocarbons), was eluted with hexane, and the other neutral fractions (N2: ketones, esters and aromatics, N3: alcohols, N4: polar compounds) sequentially eluted with dichloromethane, ethyl acetate:hexane (1:3, v:v) and methanol. The TAF fraction was derivatised in sealed vials using 12 % boron trifluoride in methanol at 70 °C for 1 hour to convert any n-alkanoic acids to fatty acid methyl esters (FAMEs). A final clean-up was performed using a silica gel column to purify the FAMEs; non-FAME compounds (A1 fraction) were eluted with hexane and FAME compounds (A2 fraction) were eluted with dichloromethane. The N1 and A2 fractions were prepared for analysis by dissolving in hexane, and the other fractions archived.

3.3 GC-MS and GC-FID analysis

Gas Chromatography – Mass Spectrometry (GC-MS) analysis was performed for compound identification at the University of Glasgow using an Agilent 7890B Gas Chromatogram connected to a 5977A mass spectrometer detector with an electron impact ionisation source. Analysis of 10 representative samples confirmed that the N1 and A2 fractions were dominantly comprised of n-alkanes and n-alkanoic acids (as FAMEs), respectively (Appendix A). N-alkane and FAME concentrations were then determined using an Agilent 7890B Gas Chromatogram fitted with a flame ionisation detector (GC-FID). For full GC-MS and GC-FID instrument settings, see Rex et al. (2023a, preprint). The A2 fraction was analysed in 200 µL of hexane, and the N1 fraction in 100 µL to 200 µL, depending on yield. For each sample a volume of 1 µL was injected. Peak areas of the C_{15} – C_{33} n-alkanes and C_{14} – C_{32} n-alkanoic acids were converted to concentrations via a set of external calibrations using a standard mix of eleven n-alkanes (following Rex et al., 2023a, preprint) at three concentrations (2.5 µg/mL, 5 µg/mL and 10 µg/mL). Concentrations for peaks with a 0 – 25 minute, 25 – 35 minute and 35 – 60 minute retention time were respectively calculated from calibrations based on the C_{16}, C_{29} and the C_{39} homologues in the standard ($R^2 > 0.99$). Finally, homologue concentrations were normalised to dry sediment mass. The concentration of the C_{22} n-alkanoic acid was not measured for all samples due to the presence of phthalate compound peaks at a similar retention time (~34.5 minutes) to this homologue in 38 % of samples (Appendix A). The n-alkane concentrations were then used to quantify a range of indices of environmental change. These were the short-chained Carbon Preference Index ($CPI_{15\text{-}20}$; Equation 1), long-chained Carbon Preference Index ($CPI_{27\text{-}32}$; Equation 2), Terrestrial to Aquatic Ratio (TAR; Equation 3) and the Average Chain Length ($ACL_{15\text{-}33}$; Equation 4). $CPI_{15\text{-}20}$ and $CPI_{27\text{-}32}$ are indicators of both source and preservation, whereas TAR and $ACL_{15\text{-}33}$ can be used to distinguish between terrestrial and aquatic sources (Zhang et al., 2020), and hence these indices can be used to reconstruct lacustrine development. The n-alkane concentrations were used instead of the n-alkanoic acid concentrations, despite the latter being higher, because n-alkanoic acids more easily degrade (Meyers and Ishiwatari, 1993) and hence these indices (particularly the CPI values) could be affected by preservation as well as environmental changes.

$$CPI_{15\text{-}20} = \frac{([C_{15}] + [C_{17}] + [C_{19}])}{([C_{16}] + [C_{18}] + [C_{20}])}$$

Equation 1 (Zhang et al., 2020)

$$CPI_{27\text{-}32} = \frac{([C_{27}] + [C_{29}] + [C_{31}])}{([C_{28}] + [C_{30}] + [C_{32}])}$$

Equation 2

$$TAR = \frac{([C_{29}] + [C_{31}] + [C_{33}])}{([C_{15}] + [C_{17}] + [C_{19}])}$$

Equation 3 (Zhang et al., 2020)

$$ACL_{15\text{-}33} = \frac{(15[C_{15}] + 17[C_{17}] + 19[C_{19}] + 21[C_{21}] + 23[C_{23}] + 25[C_{25}] + 27[C_{27}] + 29[C_{29}] + 31[C_{31}] + 33[C_{33}])}{([C_{15}] + [C_{17}] + [C_{19}] + [C_{21}] + [C_{23}] + [C_{25}] + [C_{27}] + [C_{29}] + [C_{31}] + [C_{33}])}$$

Equation 4 (Zhang et al., 2020)

3.4 GC-IRMS analysis

The compound-specific hydrogen isotope (δ^2H) composition of the C_{26}, C_{28} and C_{30} n-alkanoic acids as FAMEs ($\delta^2H_{C26acid}$, $\delta^2H_{C28acid}$ and $\delta^2H_{C30acid}$) were measured at Hokkaido University. The n-alkanoic acids were selected for this purpose to be consistent with previous analysis on the Suigetsu cores (Rex et al., 2023a, preprint) and because δ^2H analysis of the n-alkanes was prohibited by low homologue concentrations. Similarly, the aquatic n-alkanoic acid homologues were also too low in concentration to analyse. The Results section below considers the effect of n-alkanoic acid degradation on the δ^2H_{acid} values. Analysis was performed using an Agilent GC7890 gas chromatography (GC) system connected to an Elementar Isoprime vision isotope ratio mass spectrometer (IRMS) via a ceramic tube thermal conversion furnace. The GC employed a DB5 capillary column (60 m length, 0.25 mm internal diameter, 0.25 µm film thickness). The helium carrier gas flow rate was 1.1 mL min $^{-1}$. Each A2 fraction was dissolved in 25 – 330 µL of hexane and 0.50 – 3.90 µL injected (depending on FAME yield). The inlet was kept at 350 ^{o}C and the following oven programme used: the oven was held for 4 minutes at 50 ^{o}C and raised to 120 ^{o}C at 20 ^{o}C min^{-1}, then increased to 310 ^{o}C at 5 ^{o}C min^{-1} and held for 30 minutes. The furnace temperature was set to 1450 ^{o}C with an interface temperature of 350 ^{o}C. In samples containing a contaminant phthalate peak, flow was redirected to prevent entry of this contaminant into the IRMS. Subsamples were measured in duplicate and the δ^2H values of each homologue were calculated relative to a calibrated reference H_2 gas. These values were then converted to the VSMOW scale via a calibration to measurements of the standard n-alkane mixture A6 from Indiana University (containing C_{16} to C_{30} n-alkanes). All hydrogen isotope data are expressed in standard delta (δ) notation in per mille (‰) deviations relative to VSMOW. Analytical accuracy of the standard measurements was within 5 ‰. The H_3^+ correction factor ranged from 4 to 5. Values were corrected for the methylation process using a mass balance scheme (Chivall et al., 2012) to convert the measured FAME δ^2H values to n-alkanoic acid values (excluding the exchangeable hydrogen on the carboxylic acid group). GC-IRMS measurements of (Z)-hexadec-9-enoic acid (δ^2H = -154.02 ‰) and methyl (Z)-hexadec-9-enoate (δ^2H = -143.13 ‰) were made at the University of Glasgow to calculate the δ^2H value of a single methanol-derived methyl hydrogen (δ^2H = -37.86 ‰), which was used in the mass balance calculations. Low concentrations affected the repeatability of the measurements of $\delta^2H_{C26acid}$, $\delta^2H_{C28acid}$ or $\delta^2H_{C30acid}$ in 11 samples; these were therefore excluded from the final dataset. In 5 samples it was not possible to accurately measure δ^2H_{acid} for any of the three homologues. The mean precision of the δ^2H_{acid} measurements was ± 2.5 ‰ (1σ range). The final dataset comprises 44 datapoints for the $\delta^2H_{C26acid}$, 49 for $\delta^2H_{C28acid}$ and 33 for $\delta^2H_{C30acid}$.

4.0 Results

4.1 Lipid concentration and index variations

Down-core fluctuations of measured n-alkane and n-alkanoic acid concentrations and n-alkane indices provide information on the evolution of the Lake Suigetsu catchment across TII and constrain the most significant shifts in catchment development to between ~131.0 ka BP and ~129.8 ka BP (Figure 3). These observations support existing TOC/TN, $\delta^{13}C_{org}$ and diatom species variations across the interval (Francke et al., in prep; Saito-Kato et al., in prep). Terrestrial (long-chained, $\geq C_{26}$) n-alkane and n-alkanoic acid homologue concentrations were generally greater and more variable prior to 129.7 ka BP (<22.0 μg g^{-1} for the n-alkanes, <58.0 μg g^{-1} for the n-alkanoic acids); after this, the concentrations of both were low and stable (<1.1 μg g^{-1} for the n-alkanes, <20.4 μg g^{-1} for the n-alkanoic acids). N-alkanoic acid concentrations were generally greater than the concentration of the n-alkanes for similar chain lengths (e.g., a mean concentration of 6.7 μg g^{-1} for the C_{30} n-alkanoic acid, and 2.6 μg g^{-1} for the C_{29} n-alkane), and the concentrations of the C_{26} and C_{28} n-alkanoic acid homologues were consistently the largest. The concentration of the terrestrial n-alkane homologues decreased abruptly at 130.9 ka BP, whereas the concentration of the terrestrial n-alkanoic acid homologues decreased later at 129.7 ka BP. Only very small fluctuations (on the order of ~10 μg g^{-1}), limited to the terrestrial n-alkanoic acid concentrations, were observed later in the profile (127.2 ka BP onwards). Aquatic (short-chained, $\leq C_{19}$) n-alkane concentrations were generally very low; values were slightly elevated prior to 131.0 ka BP, particularly the C_{19} homologue, however the difference between these earlier values and the remainder of the profile was <1.8 μg g^{-1} (i.e., negligible). The aquatic n-alkanoic acid concentrations were more distinct by comparison; whilst the concentration of the C_{14} n-alkanoic acid changed minimally across the study interval, there were peaks with values up to ~8 µg g^{-1} larger than the interval mean C_{16} and C_{18} n-alkanoic acid concentration between ~130 and 128 ka BP.

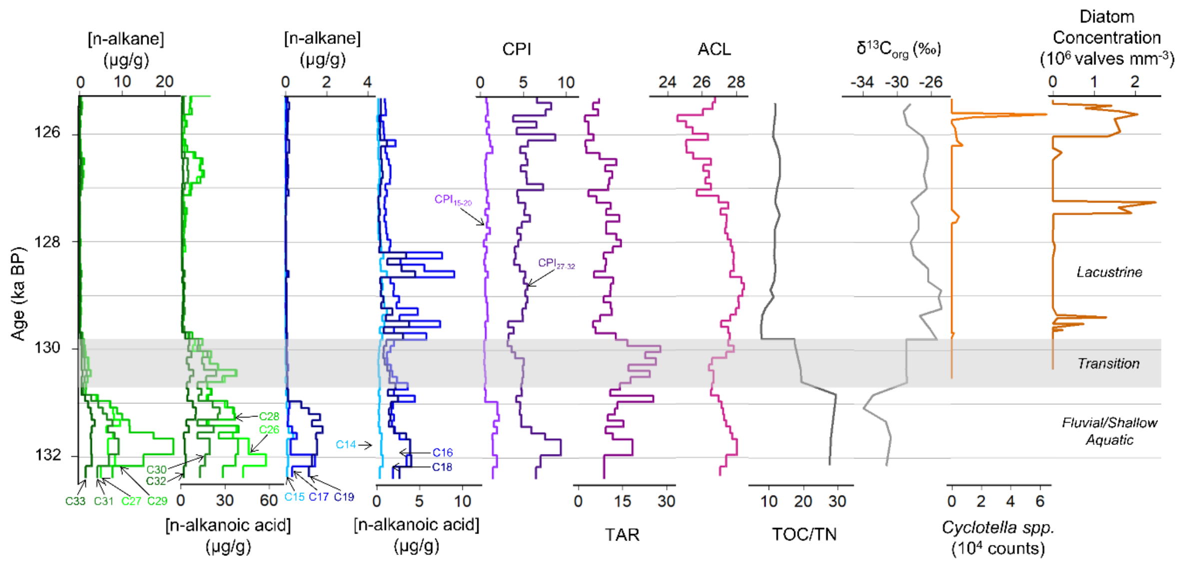

Figure 3 – Evidence for catchment evolution at Lake Suigetsu during Glacial Termination II. Panels show mass-normalised n-alkane and n-alkanoic acid concentrations of key terrestrial (green) and aquatic (blue) chain lengths, short- and long-chained n-alkane Carbon Preference Indices (CPI), n-alkane Terrestrial to Aquatic Ratio (TAR), n-alkane Average Chain Length (ACL_{15-33}), ratio of Total Organic Carbon to Total Nitrogen (TOC/TN; Francke et al., in prep), carbon isotope ratio of organic matter ($\delta^{13}C_{org}$; Francke et al., in prep), counts of brackish-tolerant *Cyclotella* spp. diatoms (Saito-Kato et al., in prep) and diatom frustule concentrations (Saito-Kato et al., in prep). See methods for concentration and index calculations. The grey horizontal bar indicates the key environmental transition based on the data.

The short-chained Carbon Preference Index (CPI_{15-20}) values ranged from 0.39 to 2.18 with a mean of 0.88, representing very minimal fluctuations with time. Contrastingly, the long-chained CPI (CPI_{27-32}) were more variable, but exhibited consistently higher values (3.14 to 9.39, mean 5.19). The greatest CPI_{27-32} values were observed prior to 131.5 ka BP and post-127.0 ka BP. The Terrestrial to Aquatic ratio (TAR) increased from the start of the study interval to 130.0 ka BP (reaching a maximum of 28.0), before rapidly decreasing over a 300-year interval and subsequently fluctuating about a mean of 8.2 between 129.7 and 125.2 ka BP. Across the entire interval, the mean Average Chain Length (ACL_{15-33}) was 27.0, oscillating minimally from 132.7 to 127.2 ka BP before decreasing slightly and exhibiting greater variability to 125.2 ka BP. The bulk TOC/TN ratio and $\delta^{13}C_{org}$ displayed inverse behaviour, with the former exhibiting higher values (>20) prior to 131.0 ka BP and decreasing across a 1.2 ka interval to lower values (~10), and the latter exhibiting lower values (-30 to -34 ‰) before increasing to a mean of 27 ‰ (Francke et al., in prep). Incursions of (brackish-tolerant) *Cyclotella spp.* occurred at 129.7, 127.5, 126.1 and 125.6 ka BP, coinciding with increases in diatom frustule concentration (Saito-Kato et al., in prep).

4.2 Catchment evolution

Our observations align with the interpretation of lake evolution presented by Francke et al. (in prep); prior to 131.0 ka BP, the area was dominated by a varying fluvial system interspersed with shallow water and peat bog environments, which gradually evolved into a productive lacustrine system. This process occurred over a ~1.2 ka interval. Observations prior to 131.0 ka BP (higher terrestrial n-alkane and n-alkanoic acid homologue concentrations, TAR values, TOC/TN ratios and $\delta^{13}C_{org}$ values, and lower aquatic n-alkanoic acid homologue concentrations), further reinforced by the presence of frequent, thick peat-rich layers, are consistent with a shallow/semi-aquatic setting, with significant amounts of terrestrially-sourced organic inputs and limited aquatic productivity. Conversely, after 129.8 ka BP, our analyses indicate lower terrestrial n-alkane and n-alkanoic acid homologue concentrations, TAR values, TOC/TN ratios and $\delta^{13}C_{org}$ values, as well as significant peaks in aquatic n-alkanoic acid homologue and diatom frustule concentrations. These younger sediments are richer in clays and increasingly laminated, implying that there was an increase in aquatic influence (and greater aquatic productivity), which likely resulted from the establishment of a lacustrine system.

Interestingly, some variables exhibited gradual shifts between 131.0 and 129.8 ka BP (including the terrestrial n-alkane and n-alkanoic acid homologue concentrations), however, the changes in the aquatic n-alkanoic acid concentrations and TAR values occurred abruptly at ~129.8 ka BP, coinciding with a significant decrease in the TOC/TN ratio and $\delta^{13}C_{org}$. This suggests that whilst terrestrial influence decreased slowly across the transition from a shallow/semi-aquatic to a lacustrine environment, aquatic productivity may have exhibited some sort of threshold behaviour because it intensified rapidly (on the order of a hundred years). This abrupt shift in aquatic productivity could be due to a water depth threshold being exceeded, likely assisted by tectonic subsidence (and an increase in precipitation, discussed in Section 4.5). Whilst the gradual decrease in terrestrial influence could indicate a reduction in the influence of surrounding vegetation, we instead attribute this to decreasing quantities of peat at the coring site (and hence lower TOC values post-transition). Indeed, the consistently high CPI_{27-32} and ACL_{15-33} values support the notion that terrestrial influence on the lake system after 129.8 ka BP was still much greater than the aquatic. The dominance of the terrestrial component appears to be an intrinsic characteristic of biomarkers from the Lake Suigetsu sediment cores, consistent with observations of materials from TI (Rex et al., 2023a, preprint). Whilst the CPI_{15-25} values were consistently low (indicative of degradation), we attribute this to very low short-chained n-alkane homologue concentrations (close to the limit of detection), rather than poor preservation (Lupien et al., 2022), although this value (~1) could indicate a microorganism source (Zhang et al., 2020). The CPI_{27-32} values do not suggest degradation of the long-chained n-alkane homologues because these values were significantly larger than 1. Instead, these values are consistent with a terrestrial source.

Whilst the initial increase in diatom frustule concentration supports the establishment of a lacustrine environment at Lake Suigetsu, diatoms were not consistently present in the core across TII; unlike TI, where diatoms were found in exceptionally high concentrations. This could indicate that the lake was only transiently suitable for diatom bloom development, or that the lake chemistry was not compatible with good diatom preservation. Slightly lower $ACL_{15\text{-}33}$ values were observed in the latter stages of TII, when the diatom frustule concentration was higher, suggesting that aquatic productivity was greater at this time. The sudden increase in the number of *Cyclotella* spp. diatoms post-126 ka BP suggests some seawater incursion during this interval. It is estimated that Lake Suigetsu was situated a few metres above sea level for the last glacial-interglacial cycle (the lake is currently at an elevation of 0 m.a.s.l. and was ~3 m.a.s.l. before the 1664 CE Kanbun Earthquake; Staff, 2011), making seawater incursions during a global highstand possible. Despite significant quantities (>10,000 counts) of *Cyclotella spp.* diatoms being observed for only ~100 years, this likely represents a continuous occurrence, disguised by non-continuous sampling and diatom preservation (Saito-Kato et al., in prep).

4.3 δ^2H_{acid} variations

Profiles of δ^2H_{acid} across TII derived from the three key terrestrial homologues ($\delta^2H_{C26acid}$, $\delta^2H_{C28acid}$ and $\delta^2H_{C30acid}$) share many key features (Figure 4), however some differences between homologue compositions are observed. From 132.7 ka BP to 130.1 ka BP, the δ^2H_{acid} values were variable and fluctuated on a centennial scale; during this interval the $\delta^2H_{C30acid}$ values were often higher than the other homologues (up to as -147 ‰, akin to later in the study period). From 130.1 to 129.2 ka BP, all of the δ^2H_{acid} values increased significantly (equating to a change of +93 ‰ in $\delta^2H_{C28acid}$) and, for the most part, smoothly, aside from a singular, large, sub-100-year positive excursion observed in $\delta^2H_{C26acid}$ and $\delta^2H_{C28acid}$. The δ^2H_{acid} values then exhibited an interval of stable, intermediate values (between 129.1 and 128.7 ka BP, with a mean composition of -172 ‰). Between 128.7 and 128.1 ka BP, $\delta^2H_{C26acid}$ and $\delta^2H_{C28acid}$ rapidly increased and then slowly decreased. This was an interval not constrained by many reliable measurements of δ^2H_{acid}, however these observations are based on bracketing measurements and a measurement of $\delta^2H_{C28acid}$ mid-transition. Post-128.1 ka BP, all of the δ^2H_{acid} values increased gradually, exhibiting some (multi-)centennial variability. The largest deviations from the overall trend in this interval were exhibited by the $\delta^2H_{C26acid}$ values, which displayed generally lower values than the C_{28} and C_{30} homologues.

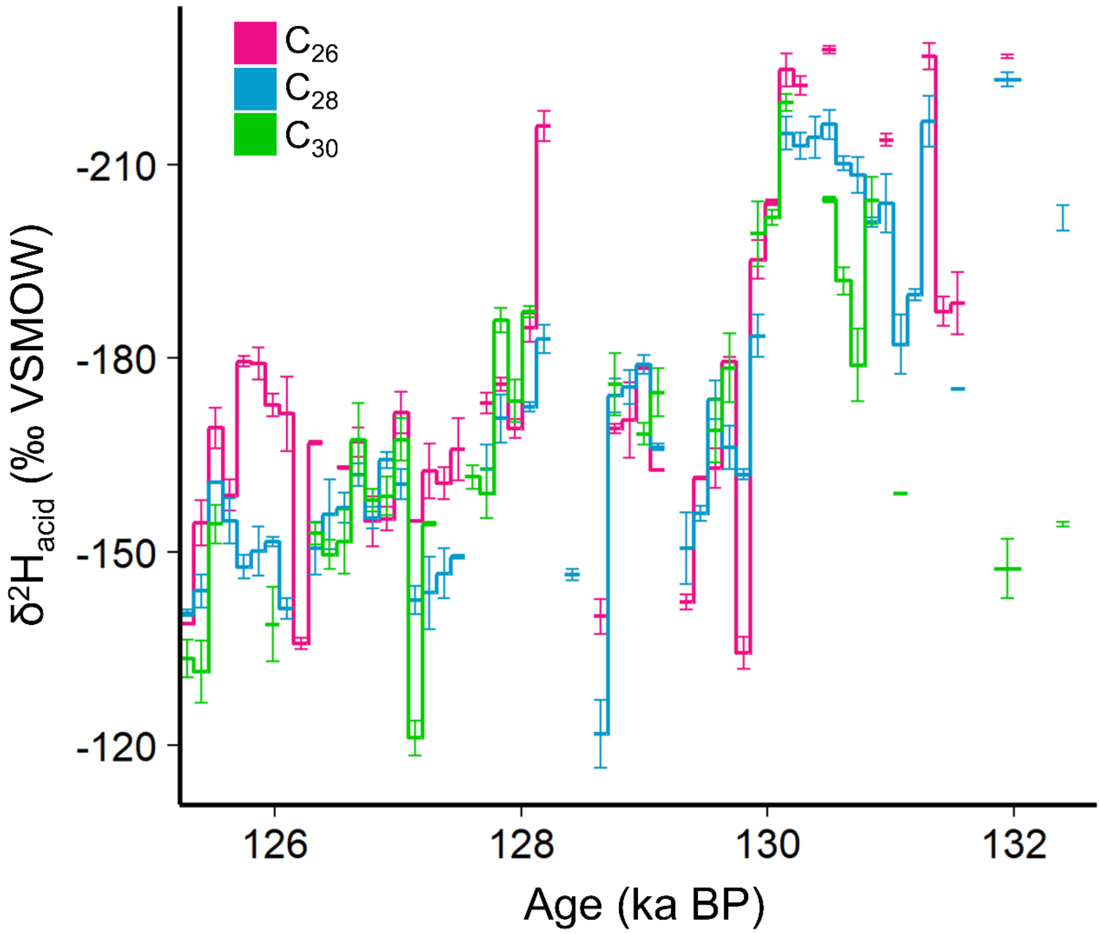

Figure 4 – δ^2H derived from the C_{26}, C_{28} and C_{30} n-alkanoic acid homologues during TII at Lake Suigetsu. Error bars show a 1σ range. The vertical axis is shown inverted such that the values reflect increasing depletion of deuterium (i.e., a stronger EASM; see below for signal interpretation).

4.4 Signal interpretation

It is vital to carefully consider the drivers of δ^2H_{acid} in order to make robust links between this variable and regional scale hydrological behaviours, particularly within a catchment under the influence of a highly seasonal climate regime. δ^2H_{acid}, like the hydrogen isotope composition of other lipid biomarkers, is closely related to the δ^2H of soil pore water, which is principally controlled by the δ^2H of precipitation ($\delta^2H_{precipitation}$) (Sachse et al., 2012). It is this relationship which facilitates the use of δ^2H_{acid} as a tracer for shifts in atmospheric circulation and vapour transport (Tierney et al., 2008). Within the context of the Lake Suigetsu catchment, modern monitoring has demonstrated that extended modes of precipitation, including the EASM, dominate the delivery of freshwater (and hence water isotopes) to the area (Rex et al., 2023b, preprint). Previous analysis of δ^2H_{acid} from the Suigetsu cores found the most robust links between this variable and EASM behaviour were established using $\delta^2H_{C30acid}$ (Rex et al., 2023a, preprint), due to the strictly terrestrial source of the C_{30} n-alkanoic acid homologue (circumventing the influence of the catchment transit lag (Rex et al. 2023b, preprint)) and the weighting of $\delta^2H_{C30acid}$ to summer $\delta^2H_{precipitation}$ (because leaf wax production occurs during the summer growth season). Contrastingly, $\delta^2H_{C26acid}$ and $\delta^2H_{C28acid}$ exhibited slightly more aquatic character and hence were influenced by $\delta^2H_{precipitation}$ from other seasons (namely the EAWM) due to the mixed seasonality of lake water during the summer growth period (Rex et al., 2023a, preprint). This highlights the importance of developing a strong understanding of proxy seasonality to facilitate signal interpretation (Kurita et al., 2015; Rex et al., 2023b, preprint). These findings align with other studies, which found that the C_{28} n-alkanoic acid homologue can be produced within the water column in some lakes (van Bree et al., 2018) and that $\delta^2H_{C30acid}$ is derived only from higher plants and hence captures a purely terrestrial signal (Tierney et al., 2022).

We apply the same reasoning to our analysis across TII and posit that the $\delta^2H_{C30acid}$ values from Lake Suigetsu most faithfully represent a terrestrial signal with the strongest links to EASM $\delta^2H_{precipitation}$. Furthermore, the solely terrestrial source of $\delta^2H_{C30acid}$ makes it possible to assume that the aforementioned catchment variability and lake development had a negligible effect on this variable. Hence, we attribute the differences observed between the $\delta^2H_{C30acid}$ values and those derived from the shorter chained homologues to aquatic influences on the latter (either lacustrine development or mixed seasonality, or a combination of these effects). Hence, subsequent analysis focusses on the $\delta^2H_{C30acid}$ values. The C_{30} homologue was generally found to be lower in concentration than the C_{26} and C_{28} homologues, and hence produced fewer data points during δ^2H_{acid} analysis, however clear patterns could nevertheless be observed in $\delta^2H_{C30acid}$ (Figure 5). Use of the $\delta^2H_{C30acid}$ values was not prohibited by degradation; we calculated the CPI_{27-32} for each sample using the n-alkanoic acid concentrations, rearranging Equation 2 for the even-over-odd preference of n-alkanoic acids, and found that the resulting values indicated good preservation of the C_{30} n-alkanoic acid (mean 6.9; minimum 2.8). Additionally, least-squares regression analysis of these n-alkanoic acid CPI_{27-32} values and $\delta^2H_{C30acid}$ values displayed a weak correlation (R^2 = 0.27), indicating that even the small variations in the degradation of the n-alkanoic acids did not alter the $\delta^2H_{C30acid}$ values (after Lupien et al., 2022).

Despite the evidence to support a strong link between $\delta^2H_{C30acid}$ and EASM $\delta^2H_{precipitation}$ at Lake Suigetsu, it is also important to consider the influence of local processes (most crucially temperature and vegetation change) on $\delta^2H_{C30acid}$ (Holtvoeth et al., 2019). An assessment of the impact of these processes can be made by using preliminary complementary pollen analyses and pollen-derived temperature reconstructions from the cores across TII (albeit at a lower resolution than the $\delta^2H_{C30acid}$ analyses), which can assist in determining the magnitude of these alternative influences. These pollen analyses were derived following the methods presented by Nakagawa et al. (2021). The impact of vegetative change, particularly the relative amounts of C3 versus C4 plants (Tierney et al., 2010), was negligible, because the dominant species across the TII interval were trees with similar biosynthetic pathways (including *Alnus*, *Carpinus*, *Cryptomeria*, *Fagus*, *Quercus* and *Tsuga*, all of which are classified as C3 vegetation). Conversely, the impact of temperature on $\delta^2H_{C30acid}$ is more difficult to define. The pollen-reconstructed mean temperature of the warmest month (MTWA) displays some similarities to the δ^2H_{acid} profiles; it increased from 131.6 ka BP to 129.8 ka BP, decreased to 128.0 ka BP, then increased to a maximum at 126.4 ka BP (Figure 5). This trend broadly follows that of $\delta^2H_{C30acid}$ in the earlier stages of TII (pre-130.0 ka BP), before decoupling. During TI, higher resolution pollen-derived temperature analyses allowed for a confident assertion that climate (and hence vegetation change) were not significant drivers of $\delta^2H_{C30acid}$ (Rex et al., 2023a, preprint). Whilst ground-truthing these observations in a more intensely studied climatic interval provides strong evidence that the effect of temperature on $\delta^2H_{C30acid}$ was also limited during TII, it is important to note that the magnitude of change observed in $\delta^2H_{C30acid}$ was greater in TII than in TI (particularly in the pre-130.0 ka BP period), and that a qualitative relationship to temperature during this period is apparent (albeit temporally constrained). This suggests that, whilst other drivers are possible, there could be a temperature component to this signal. Whilst some studies have attributed this to the effect of regional temperature on $\delta^2H_{precipitation}$ (e.g., Thomas et al., 2014), this could also be a local effect (via greater soil evaporation and transpiration within the catchment; Sachse et al., 2012). In light of this, it is possible that a combination of decreasing $\delta^2H_{precipitation}$ and rising temperatures contributed to the initial decrease in $\delta^2H_{C30acid}$ prior to 130.0 ka BP. However, a temperature increase alone cannot account for the 72.3 ‰ decrease (maximum to minimum difference) in $\delta^2H_{C30acid}$ between the start of the record and 130.0 ka BP; the 6.7 °C temperature increase (ΔT) indicated by the pollen climate reconstruction would yield only a ~14 ‰ change in $\delta^2H_{C30acid}$, using the ΔT-$\Delta\delta^{18}O$ relationship presented by Rozanski et al. (1993) ($\Delta\delta^{18}O = 0.31\Delta T - 0.33$) and the global meteoric water line relationship between $\Delta\delta^{18}O$ and $\Delta\delta^2H$ ($\Delta\delta^2H/\Delta\delta^{18}O = 8$). Hence, there must also be a change in $\delta^2H_{precipitation}$ during this interval. Additionally, the relationship between $\delta^2H_{C30acid}$ and temperature breaks down post-130.0 ka BP, suggesting that for the remainder of TII, the $\delta^2H_{C30acid}$ values were dominantly driven by $\delta^2H_{precipitation}$ alone.

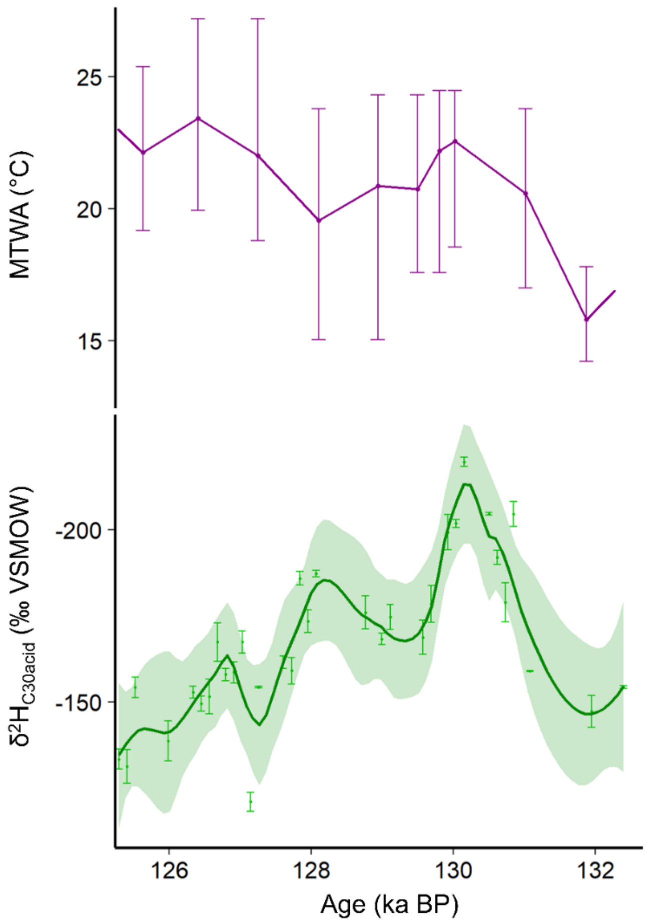

Figure 5 – $\delta^2H_{C30acid}$ and pollen-derived temperature evolution during TII at Lake Suigetsu. The lower panel shows the evolution of δ^2H_{acid} derived from the C_{30} n-alkanoic acid homologue. Individual data points with 1σ error bars are shown, overlying a loess-smoothed trendline (span = 0.25) with 1σ confidence bands. The vertical axis is shown inverted such that the values reflect increasing depletion of deuterium (i.e., a stronger EASM; see below for signal interpretation). The upper panel shows the pollen-derived mean temperature of the warmest month (MTWA) with error bars showing minimum/maximum values inferred for the same interval. Timescales are equivalent because both sets of analyses were performed on the SG06 core.

4.5 EASM evolution

The EASM system is driven by a series of interconnected climate features, centred around the northwards propagation of the EASM front, which is propagated by the position and intensification of the Western Pacific Subtropical High (Kurita et al., 2015; Xu et al., 2020). It follows that modifications to this scheme which alter EASM strength are the dominant controls on $\delta^2H_{C30acid}$ across much of TII, with an additional temperature component in the pre-130 ka BP interval. Like across TI, we suggest that EASM $\delta^2H_{precipitation}$ is controlled by a combination of source composition and transport processes, and that a "stronger" EASM would have lower $\delta^2H_{preciptation}$ (and hence $\delta^2H_{C30acid}$) values due to stronger winds and greater quantities of precipitation integrated across the transport pathway (Rex et al., 2023a, preprint). Kurita et al. (2015) found a strong inverse relationship between contemporary EASM strength and $\delta^2H_{precipitation}$ in Tokyo, Japan, which supports the notion that $\delta^2H_{C30acid}$ is related to EASM evolution.

Based on these assertions, our record supports EASM strengthening from the start of TII in the penultimate glacial period to ~130 ka BP (alongside an increase in temperature), before rapid weakening to 129.5 ka BP. There is also some evidence for subsequent strengthening to 129.0 ka BP, albeit more gradual than indicated by $\delta^2H_{C26acid}$ and $\delta^2H_{C28acid}$, followed by continued weakening into the last interglacial period. Interestingly, the most significant period of EASM strengthening during TII occurred immediately prior to, and during, the transition from shallow/semi-aquatic to lacustrine conditions at the catchment between 131.0 and 129.8 ka BP. As mentioned above, it is unlikely that this catchment evolution affected $\delta^2H_{C30acid}$, which is derived from terrestrial plants, effectively decoupling this variable from lake behaviours. However, it is possible that this increase in EASM strength also increased freshwater delivery to the area, contributing to lake system formation, alongside tectonic subsidence.

5.0 Discussion

5.1 A note on chronological alignment

Our results support an initial increase in EASM strength in Japan during MIS 6, which reached a maximum at ~130 ka BP, followed by overall weakening with some evidence for submillennial-scale variability (weakening to 129.5 ka BP, strengthening to 129.0 ka BP and then weakening into MIS 5e). Comparing this behaviour to other key regional records of temperature and EASM strength is important for an integrated understanding of EASM evolution across TII. However, chronological alignment across TII is more challenging than for more recent intervals, because many archives (including Lake Suigetsu) lack independent chronologies and hence age control is often obtained by tuning to other sites (sometimes via climate parameters). A conservative approach is therefore required to avoid circular reasoning, and here we present each record on their own chronology solely for orientation. This is also prudent because many archive chronologies are associated with large amounts of error (on the order of a thousand years) and hence distinguishing offsets between shifts in different regions is not practical. However, this does not prevent worthwhile comparisons being made between the structure of records from different archives.

5.2 Comparison to continental EASM records

Comparison of our $\delta^2H_{C30acid}$ EASM reconstruction to other records from the EASM region supports the notion of a "Weak Monsoon Interval" during MIS 6, and that TII was associated with EASM strengthening, however there are clear differences between records, which adds credence to previous assertions that EASM evolution during TII was extremely spatially heterogenous (Figure 6; Xue et al., 2019). Indeed, none of the records presented in Figure 6 show the same trends across this interval, aside from perhaps Sanbao Cave and Hulu Cave $\delta^{18}O_{speleothem}$, although the latter record does not extend past 128 ka BP (U-Th timescale). A common feature of some of the Chinese speleothem records is a rapid increase in EASM strength at ~129 ka BP (U-Th timescale), which was not observed at Lake Suigetsu. Accounting for chronological uncertainty, the largest increase in EASM strength observed at Lake Suigetsu (between ~131 and 130 ka BP, SG timescale) could be equivalent to this rapid shift in $\delta^{18}O_{speleothem}$; however, the shift in Suigetsu $\delta^{2}H_{C30acid}$ is more similar in duration to the gradual decrease in $\delta^{18}O_{speleothem}$ observed at Hulu Cave and Shangxiaofeng Cave. This observation contradicts previous assertions that the rapidity of the transition in $\delta^{18}O_{speleothem}$ was an indicator of EASM threshold behaviour (Yuan et al., 2004; Kelly et al., 2006), and instead suggests that, in Japan at least, EASM strengthening was a slow response to climate forcing.

Not only is the trend in EASM strength during TII at Lake Suigetsu different from other records from across the region, but so is its apparent relationship with temperature evolution. EASM strength tracks the increase in temperature at Lake Suigetsu prior to 130 ka BP, before fully decoupling from temperature, which continues to rise whilst the EASM exhibits a weakening trend (Figure 5, Figure 6). Instead of this behaviour, analysis of sediments from the South China Sea found that EASM strengthening lagged behind the temperature increase (He et al., 2017). Furthermore, EASM strength and temperature were decoupled at Xinglong Cave during the early stages of TII before coupling later on (i.e., the reverse of the trends seen at Lake Suigetsu; Duan et al., 2022). Interestingly, the temperature evolution at Lake Suigetsu and Xinglong Cave exhibit similar structural features (accounting for chronological uncertainty; Figure 6). However, whilst our EASM record at Lake Suigetsu indicates strengthening with the first rise in temperature, the increase in EASM strength at Xinglong Cave does not occur until the second temperature rise, 4 ka later.

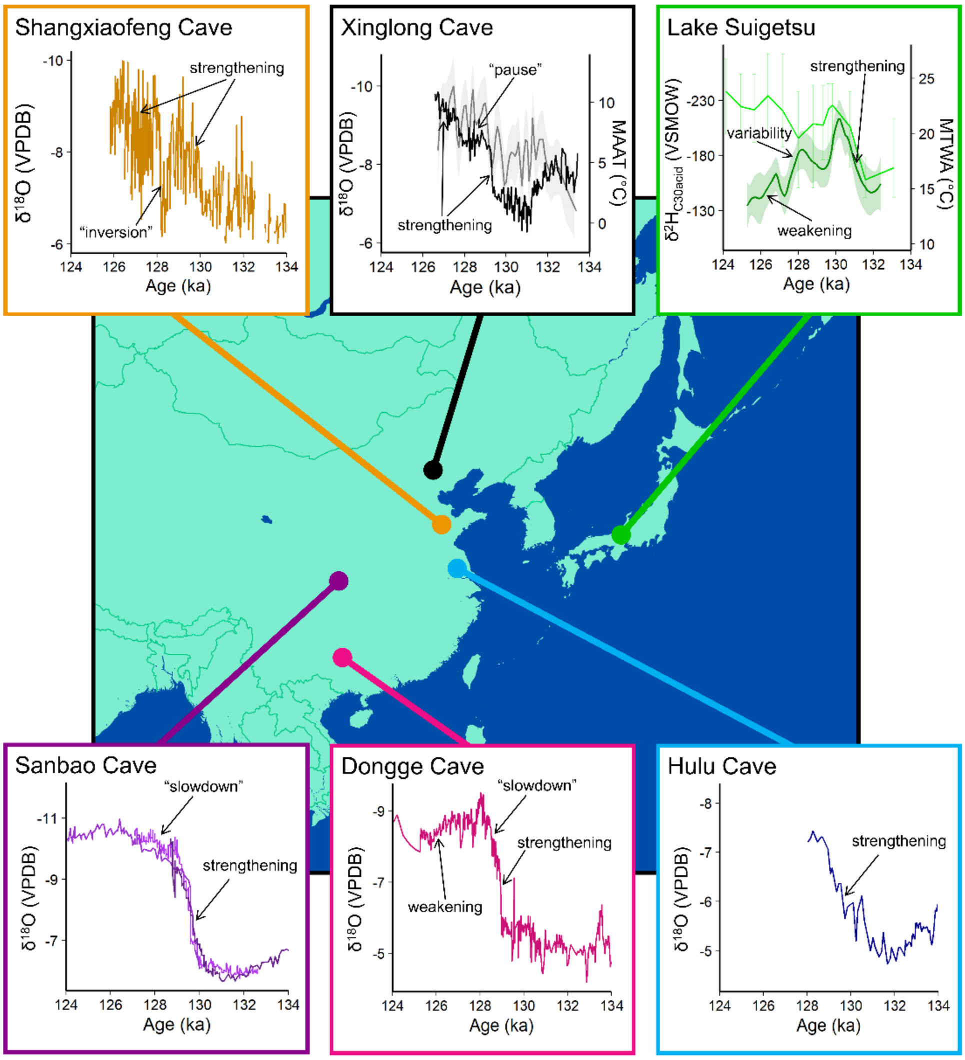

Figure 6 – Records of EASM strength between 134 and 124 ka BP and location indicators. From top left to bottom right: Shangxiaofeng Cave SD1 $\delta^{18}O_{speleothem}$ (U-Th timescale; Xue et al., 2019), Xinglong Cave XL-4 $\delta^{18}O_{speleothem}$ in black and loess-smoothed mean annual average temperature (MAAT; span = 0.1) with 1σ confidence bands in grey (U-Th timescale; Duan et al., 2019; Duan et al., 2022), loess-smoothed Lake Suigetsu SG06 $\delta^{2}H_{C30acid}$ (span = 0.25) with 1σ confidence bands in dark green and MTWA with error bars showing minimum/maximum values in light green (SG timescale; this study); Sanbao Cave SB25-2, SB23 and SB11 $\delta^{18}O_{speleothem}$ (U-Th timescale; Wang et al., 2008), Dongge Cave D4 $\delta^{18}O_{speleothem}$ (U-Th timescale; Kelly et al., 2006), Hulu Cave MSX $\delta^{18}O_{speleothem}$ (U-Th timescale; Cheng et al., 2006).

This suggests that even though quantitative comparison of these records is prohibited by circular reasoning, by assuming that the temperature variations occurred synchronously between these two sites (which is not only reasonable based on similarities in structure, but also based on observations across TI which found that temperature is likely to conform to regional/hemispheric trends), we can propose that the most significant shift in EASM strength at Lake Suigetsu occurred prior to the largest shift at Xinglong Cave (at ~129 ka BP; a sudden change common to all of the Chinese speleothem records). However, the smaller, earlier shift in Xinglong Cave (termed the "Weak Monsoon Interval Interstadial" by Duan et al. (2019)) could be equivalent to the largest shift at Lake Suigetsu, because this occurs during the first period of rising temperatures. This suggests that not only did the EASM strengthen more slowly in Japan than many parts of continental China (where records exhibit a step-change in EASM strength), but also that this strengthening occurred earlier; although without robust independent chronologies this remains tentative. It follows that EASM strengthening in Japan does not lag regional temperature increases.

Another key aspect of EASM evolution which differs between sites is the presence (or absence) of submillennial-scale variability during TII. Comparison of the Lake Suigetsu record to these other (speleothem) records is difficult due to critical structural differences (i.e., a lack of rapid strengthening at 128 ka BP (U-Th timescale). However, much like the Shangxiaofeng Cave $\delta^{18}O_{speleothem}$ record, the Suigetsu $\delta^{2}H_{C30acid}$ record provides evidence for inversions in EASM strength after an initial increase. Such features are not universally observed; there are contrasting observations from across the monsoon region as to their nature (a true "inversion", a "pause", or a "slowdown"; Figure 6). Regardless, the evidence from Suigetsu is that there was indeed some submillennial-scale variability in EASM strength during TII, in contrast to observations at Hulu and Sanbao caves (Cheng et al., 2006; Wang et al., 2008). It is interesting to note that the amplitude of millennial-scale variability observed is greater in the reconstructions derived from the most northerly archives (Shangxiaofeng Cave, Xinglong Cave and Lake Suigetsu; discussed further in Section 5.5 below).

5.3 Contrasting EASM evolution in Japan during TI and TII

The interpretation of these patterns can be assisted by comparing the findings presented here to EASM and temperature variations across TI. This exercise highlights significant differences between deglacial monsoon behaviours during these intervals (Figure 7); whilst Suigetsu pollen-derived temperature during TI and TII shows some similar character, observations of $\delta^2H_{C30acid}$ suggests unique trends in EASM strength. This is not surprising, given how other records from across the EASM region exhibit different EASM behaviours during TI and TII (e.g., Cheng et al., 2006; Duan et al., 2019). Not only is the range of Suigetsu $\delta^2H_{C30acid}$ values greater across TII than TI, suggesting higher amplitude changes in EASM strength (accounting for a contribution to $\delta^2H_{C30acid}$ from rising temperatures, as mentioned previously), but there are limited similarities in structure.

Other reconstructions have suggested that EASM change appears to lag behind many other significant climatic shifts during TII (including increasing southern hemisphere temperature, global carbon dioxide concentration and initial increases in methane concentration; Yuan et al., 2004). These studies instead aligned the increase in EASM strength to Northern Hemisphere temperatures (Masson-Delmotte et al., 2010; Li et al., 2014). Under these circumstances, EASM strengthening would denote the full inception of global interglacial conditions (Yuan et al., 2004; Kelly et al., 2006). Wang et al. (2008) suggested that this delay to EASM strengthening was due to the persistence of cold conditions during Heinrich Event 11 in the North Atlantic, which suppressed AMOC and forced the Intertropical Convergence Zone (ITCZ) to the south, a key component of the argument for an EASM-North

Atlantic teleconnection during TII (Xue et al., 2019). However, our record from Lake Suigetsu suggests that EASM strengthening in Japan occurred prior to this, challenging this North Atlantic-centric viewpoint and allowing for alternative teleconnections and forcing mechanisms to be explored.

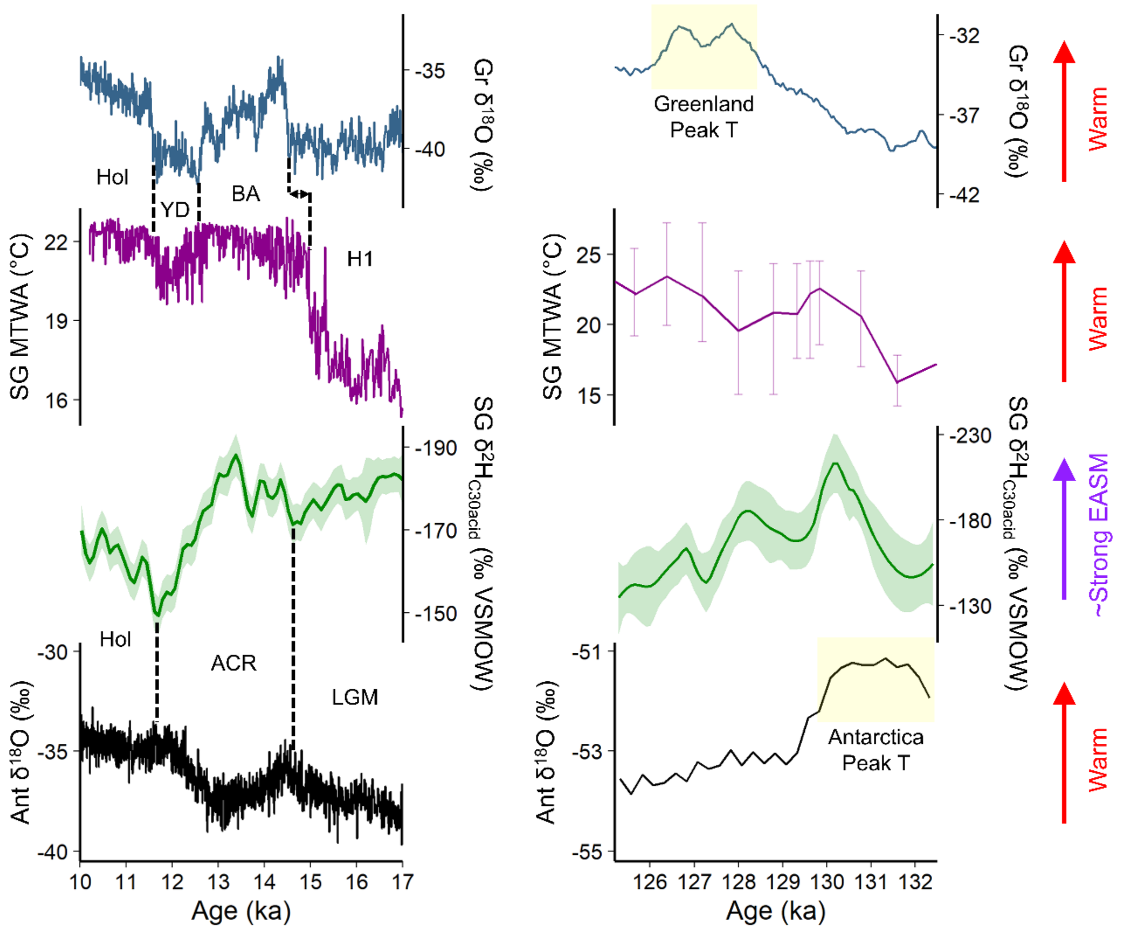

Figure 7 – Comparison of records from Greenland (Gr), Lake Suigetsu (SG) and Antarctica (Ant) during TI and TII. TI records: GRIP $\delta^{18}O_{ice}$ (Johnsen et al., 1997; Rasmussen et al., 2014; remodelled onto the U-Th timescale as per Rex et al., 2023a, preprint), Suigetsu mean temperature of the warmest month (MTWA; Nakagawa et al., 2021; IntCal20 timescale), loess-smoothed Suigetsu $\delta^2H_{C30acid}$ (span = 0.1) with 1σ confidence bands (EASM proxy; Rex et al., 2023a, preprint; IntCal20 timescale), Antarctica WAIS Divide $\delta^{18}O_{ice}$ (WAIS Divide Project Members, 2013; WD2014 timescale). TII records: Synthetic Greenland $\delta^{18}O_{ice}$ (Barker et al., 2011; EDC3 timescale), Suigetsu MTWA with error bars showing minimum/maximum values (this study; SG timescale), loess-smoothed Suigetsu $\delta^2H_{C30acid}$ (span = 0.25) with 1σ confidence bands (this study; SG timescale), Antarctica Dome Fuji $\delta^{18}O_{ice}$ (DFO-2006 age) (Kawamura et al., 2007). (colour figure)

EASM strength in Japan across TI displayed an inverse response to the ACR (Rex et al., 2023a, preprint), whereas pollen-derived temperature was closely related to Greenland (i.e., North Atlantic) temperature (albeit with an earlier late glacial interstade onset (Nakagawa et al., 2021)). Rex et al. (2023a, preprint) proposed that insolation was the key driver of EASM strengthening across TI on multi-millennial timescales but attributed the propagation of an inverse response to the ACR to Pacific climate variability. It was suggested that the preservation of these Antarctic signals was enhanced by Japan's location at a higher latitude, adjacent to the Pacific regime and isolated from mainland China. Applying these principles to our interpretation of EASM variability during TII can help to rationalise our observations from Lake Suigetsu.

5.4 Climate forcing

The most likely driver of EASM variability during TII is Northern Hemisphere summer insolation. The relationship between the EASM and insolation is well-established on orbital timescales (Kelly et al., 2006; Cheng et al 2019) and was considered a major driver of EASM variability during TI, and we propose that this was also the case during TII. However, insolation is only one component of the global deglacial climate sequence, and other elements of the climate system (in particular, polar temperatures) can help to rationalise our observations. Across TI, aside from Southern Hemisphere stade-interstade fluctuations leading those in the Northern Hemisphere, Antarctic and Greenlandic temperatures followed similar trends, reaching a peak in the early Holocene. However, during TII, the interhemispheric temperature gradient was significantly greater due to a large (up to 2 ka) temporal offset between peak temperatures in Greenland and Antarctica (Nilsson-Kerr et al., 2019). During TI, we observed discrepancies between records from Japan and continental China when polar temperatures were decoupled during low amplitude stade-interstade fluctuations (Rex et al., 2023a, preprint); aside from these intervals, the EASM system exhibited coherent strengthening patterns. During TII, this decoupling is even more significant; stade-interstade fluctuations were extremely muted (and highly debated), and instead we observe extremely different hemispheric glacial-interglacial fluctuations. This is critical for EASM operation because perturbations in the interhemispheric temperature gradient are intrinsically linked to atmospheric circulation and ITCZ positioning, and hence have the potential to significantly alter EASM behaviour.

We propose that these different climate behaviours during TII relative to TI, combined with greater ice volumes pre-transition (during MIS 6) and more rapid deglaciation associated with a larger solar insolation change during TII (Caley et al., 2013), were the cause of the differences in the pattern and magnitude of EASM change during TI and TII at Lake Suigetsu. Furthermore, because tangible inter-regional links have been made from both Antarctic and North Atlantic temperatures to EASM behaviour during other intervals, it follows that the observed spatial heterogeneities in EASM behaviour during TII could be due to competing influences from each pole. The Suigetsu pollen-derived temperature profile shows submillennial-scale variability during TII which cannot be explained solely by a Northern Hemisphere influence (because Greenland temperature lacks significant substructure), but could be due to a combination of the temperature profiles of both poles; an earlier peak due to the insolation increase and Antarctic warming, and a later peak due to Greenlandic warming (which is also observed in South China Sea temperatures (Clemens et al., 2018). This implies that when decoupled, polar temperatures can both have a tangible effect on the mid-latitudes.

Given the evidence for an Antarctica-Japan EASM teleconnection during TI, it is not surprising that we observe the most significant shift in EASM strength in Japan during the earlier stages of TII (when the largest changes in insolation and Antarctic temperature occurs) relative to mainland China, which displayed a strong North Atlantic teleconnection during TI. Indeed, EASM evolution in Japan appears to maintain a closer relationship to Antarctic temperatures during TII. However, it is also arguable that all sites display some degree of mixed character; for example, the Weak Monsoon Interval Interstadial at Xinglong Cave, albeit more muted than the main shift, could be representative of a Pacific influence on EASM strength at this site. Site location may be a key component of the relative influence of each teleconnection; much like TI, we propose that the location of Japan makes precipitation here especially sensitive to Pacific (and ultimately, Antarctic) changes. Hulu Cave, Shangxiaofeng Cave and Lake Suigetsu are at similar latitudes and lower elevations than the other sites, as well as being located closer to the coast, and all exhibit slower increases in EASM strength. The other sites, situated further inland, display more rapid increases in EASM strength akin to threshold behaviour, possibly due to greater influences of Heinrich Event 11 (and a stronger North Atlantic teleconnection, via the westerly jet) in these areas. The relationship between the EASM in Japan and Antarctic temperature during TII was not inverse, like during the ACR, but instead likely positively related, as with the remainder of TI, suggesting that this inverse relationship was a feature of Southern Hemisphere stadial, rather than glacial, conditions. The decrease in Antarctic temperatures during the latter stages of TII might also explain EASM weakening in Japan as indicated by our $\delta^2H_{C30acid}$ record.

5.5 Submillennial variability

Our comparison of EASM evolution during TI and TII also highlights that the observed submillennial-scale variability during TII was non-analogous to TI, and hence it is important to be tentative when suggesting that such fluctuations are akin to “Younger Dryas”-type cold inversion responses. It is not possible to say whether such cold inversion responses should be anticipated pre- or post- the major transition (i.e., whether such transitions share greater character with EASM strengthening at the onset of a late-glacial interstade ("Bølling-Allerød"-type warm period) or interglacial period (Holocene)). Instead, it is more prudent to assess whether there is any substructure to these transitions, for which the Lake Suigetsu record provides supporting evidence. However, it is likely that there is still spatial heterogeneity in such variability, as well as the potential for differences between archive type. One possible mechanism to explain these fluctuations is perturbations of AMOC, however Duan et al. (2019) suggested that meltwater pulses would have a reduced effect on AMOC, which was more strongly suppressed during TII due to the greater rapidity of ice sheet collapse (Landais et al., 2013). If these climatic conditions resulted in more muted hydrological responses to small scale temperature fluctuations (which are more difficult to preserve and detect), this could explain the ambiguous evidence for such EASM variability. An alternative explanation is that more northerly sites, situated towards the edge of the EASM domain (including Shangxiaofeng Cave, Lake Suigetsu and Xinglong Cave), were more sensitive to westerly jet repositioning as a result of subtle changes to AMOC than the more southerly cave sites.

5.6 Future work

Future work should focus on growing the network of EASM records from across the region, allowing for better clarification of signal heterogeneities during TII. Of particular value to this is the inclusion of records from alternative (non-speleothem) archives to generate a more well-rounded analysis of EASM behaviours by overcoming archive-specific limitations, although the development of independent age models is challenging in these contexts. The application of other chronological techniques to non-speleothem archives should also be a focus for future development. This is especially pertinent for those archives with the potential to discern submillennial-scale fluctuations and provide robust evidence to support or refute teleconnections. A greater number of temperature reconstructions from the region would also be beneficial in order to better understand the alignment of EASM evolution with temperature and the potential for temporally-constrained teleconnections to both poles.

6.0 Conclusions

Expanding current observations of deglacial EASM variability to include extremes of temperature and a variety of boundary conditions is crucial for a more comprehensive understanding of this influential climate system. Using lipid biomarkers and hydrogen isotopes from the Lake Suigetsu sediment cores, we examined local catchment evolution and EASM behaviour during the penultimate glacial termination (Termination II). Prior to 131.0 ka BP, the Lake Suigetsu catchment consisted of a dynamic fluvial system dominated by shallow water and peat bog environments. A deep-water lacustrine system then developed in the area, becoming fully established after ~1.2 ka, possibly driven by a combination of increased freshwater input and tectonic subsidence. There is some evidence for threshold behaviour in aquatic productivity, which initiated at 129.8 ka BP. Due to its strictly terrestrial origin, our EASM reconstructions are based on the compound-specific hydrogen isotope analysis of the C_{30} n-alkanoic acid ($\delta^2H_{C30acid}$), which provided the strongest connection to the hydrogen isotope composition of summer (EASM) precipitation and would have been negligibly affected by lake development. EASM $\delta^2H_{precipitation}$ (and ultimately EASM strength) was the predominant driver of $\delta^2H_{C30acid}$ during TII, although there was some evidence to support a temperature contribution before 130.0 ka BP. Our analysis found that the EASM strengthened from 132.5 to 130.0 ka BP before weakening to 125.2 ka BP. There is evidence to support submillennial-scale variability during this weakening phase, with weakening to 129.5 ka BP, strengthening to 129.0 ka BP and then weakening to 125.2 ka BP, in contrast to some Chinese speleothem reconstructions which exhibit smooth transitions with no/limited internal structure. Our record shares some common features with other EASM reconstructions (a "Weak Monsoon Interval" during MIS 6, and strengthening across the transition), however the distinctive character in our record (and that of other records) supports extreme spatial heterogeneity in EASM strength during TII. Alignment of temperature reconstructions at Lake Suigetsu and Xinglong Cave, China, facilitate the assertion that the increase in EASM strength in Japan was earlier and slower than the largest shift in EASM strength in continental China, partially overcoming circularity in chronological alignment.

Comparison of $\delta^2H_{C30acid}$ EASM reconstructions from Lake Suigetsu during TI and TII suggest characteristically different behaviours during these intervals, attributed to different climatic sequences, greater ice volumes and more rapid deglaciation during TII. A key component of this was the decoupling of peak temperatures at the north and south poles during TII. We propose that insolation was a major driver of EASM variability during both TI and TII, but that offset glacial-interglacial fluctuations at the poles caused the much greater spatial heterogeneity in EASM evolution during TII relative to TI. Much like during TI, Japan showed greater Antarctic (Pacific) character relative to mainland China, which displayed more coeval trends with the North Atlantic. Site location appears to be a key control of whether local EASM strength more closely tracked insolation and Antarctic temperatures or North Atlantic behaviours. Similarly, greater submillennial-scale variability was observed for the most northerly sites. Ambiguity in such trends could be attributed to difficulties in detecting low amplitude fluctuations (muted as a result of extreme AMOC suppression), or because sites towards the edge of the EASM domain were more sensitive to westerly jet repositioning. Our observations of the EASM using $\delta^2H_{C30acid}$ are the first derived using stable isotope-based climate proxies from the Japanese archipelago, and future work should continue to contribute records of EASM strength and temperature from a range of locations and archive types to assist in unravelling the complexities in deglacial EASM evolution during TII.

Acknowledgments

The authors would like to acknowledge the support of the following: Vanessa Nowinski (sub-sampling of the Lake Suigetsu sediment cores), Mohammed Ali Salik (technical support), Osamu Seki (δ^2H_{acid} analysis).

Funding: The analytical work associated with this study was supported by the Quaternary Research Association (New Research Workers Award); Scottish Alliance for Geoscience, Environment and Society (Small Grants Scheme); and the School of Geographical and Earth Science, University of Glasgow. C.L.R. was supported by the NERC IAPETUS2 Doctoral Training Partnership. The Lake Suigetsu sediment core chronology extension work was supported by ARC (Australian Research Council) Discovery Project DP200101768.

Data Availability

Accompanying data can be found at https://doi.org/10.5525/gla.researchdata.1486

Appendices

Appendix A – Chromatograms

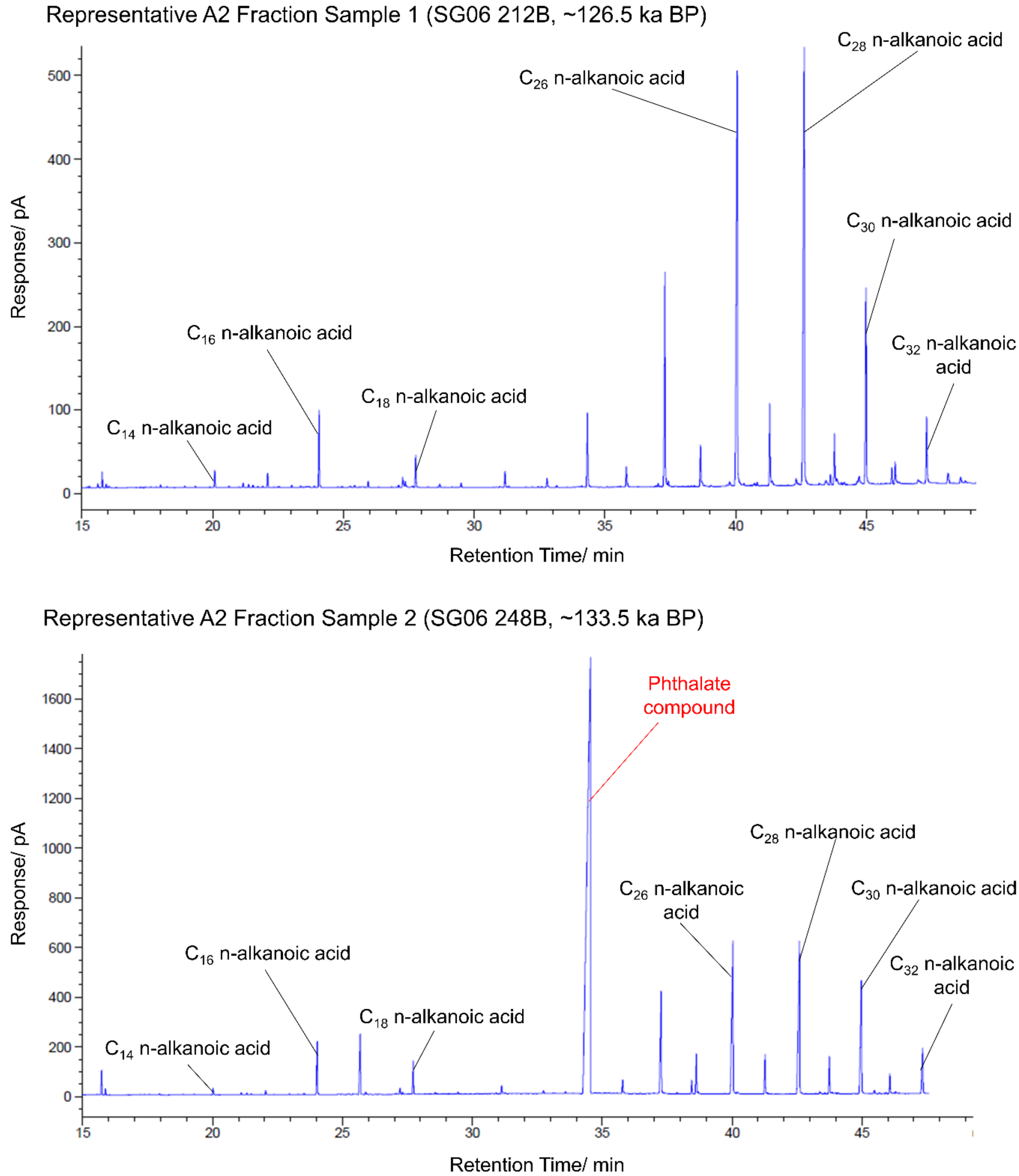

Figure A.1 – Example GC-FID A2 fraction chromatograms (method details provided in main text). Key homologue peaks are indicated. Phthalate compound peaks (lower panel) were detected in some samples but did not interfere with peaks of interest.

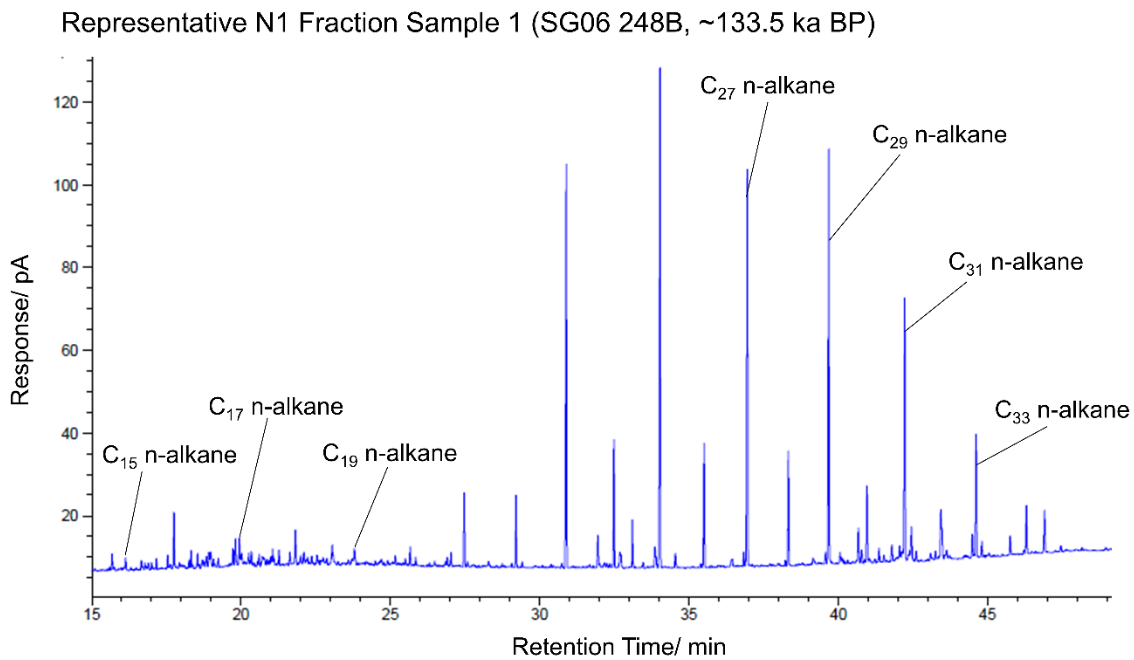

Figure A.2 – Example GC-FID N1 fraction chromatogram (method details provided in main text). Key homologue peaks are indicated.

References

Albert, P.G., Smith, V.C., Suzuki, T., McLean, D., Tomlinson, E.L., Miyabuchi, Y., Kitaba, I., Mark, D.F., Moriwaki, H., SG06 Project Members, Nakagawa, T., 2019. Geochemical characterisation of the Late Quaternary widespread Japanese tephrostratigraphic markers and correlations to the Lake Suigetsu sedimentary archive (SG06 core). Quat. Geochronol. 52, 103–131. https://doi.org/10.1016/j.quageo.2019.01.005

Barker, S., Knorr, G., 2021. Millennial scale feedbacks determine the shape and rapidity of glacial termination. Nat. Commun. 12. https://doi.org/10.1038/s41467-021-22388-6

Barker, S., Knorr, G., Edwards, R.L., Parrenin, F., Putnam, A.E., Skinner, L.C., Wolff, E., Ziegler, M., 2011. 800,000 Years of abrupt climate variability. Science. 334, 347–351. https://doi.org/10.1126/science.1203580

Broecker, W.S., Henderson, G.M., 1998. The sequence of events surrounding Termination II and their implications for the cause of glacial-interglacial CO_2 changes. Paleoceanography 13, 352–364. https://doi.org/10.1029/98PA00920

Bronk Ramsey, C., Heaton, T.J., Schlolaut, G., Staff, R.A., Bryant, C.L., Brauer, A., Lamb, H.F., Marshall, M.H., Nakagawa, T., 2020. Reanalysis of the Atmospheric Radiocarbon Calibration Record from Lake Suigetsu, Japan. Radiocarbon 62, 989–999. https://doi.org/10.1017/RDC.2020.18

Caley, T., Malaizé, B., Kageyama, M., Landais, A., Masson-Delmotte, V., 2013. Bi-hemispheric forcing for Indo-Asian monsoon during glacial terminations. Quat. Sci. Rev. 59, 1–4. https://doi.org/10.1016/j.quascirev.2012.10.008

Chen, W., Wang, L., Feng, J., Wen, Z., Ma, T., Yang, X., Wang, C., 2019. Recent Progress in Studies of the Variabilities and Mechanisms of the East Asian Monsoon in a Changing Climate. Adv. Atmos. Sci. 36, 887–901. https://doi.org/10.1007/s00376-019-8230-y

Cheng, H., Edwards, R.L., Wang, Y., Kong, X., Ming, Y., Kelly, M.J., Wang, X., Gallup, C.D., Liu, W., 2006. A penultimate glacial monsoon record from Hulu Cave and two-phase glacial terminations. Geology 34, 217–220. https://doi.org/10.1130/G22289.1

Cheng, H., Zhang, H., Zhao, J., Li, H., Ning, Y., Kathayat, G., 2019. Chinese stalagmite paleoclimate researches: A review and perspective. Sci. China Earth Sci. 62, 1489–1513. https://doi.org/10.1007/s11430-019-9478-3

Chivall, D., Berstan, R., Bull, I.D., Evershed, R.P., 2012. Isotope effects associated with the preparation and methylation of fatty acids by boron trifluoride in methanol for compound-specific stable hydrogen isotope analysis via gas chromatography/thermal conversion/isotope ratio mass spectrometry. Rapid Commun. Mass Spectrom. 26, 1232–1240. https://doi.org/10.1002/rcm.6188

Chowdary, J.S., Hu, K., Srinivas, G., Kosaka, Y., Wang, L., Rao, K.K., 2019. The Eurasian Jet Streams as Conduits for East Asian Monsoon Variability. Curr. Clim. Chang. Reports 5, 233–244. https://doi.org/10.1007/s40641-019-00134-x

Clemens, S.C., Holbourn, A., Kubota, Y., Lee, K.E., Liu, Z., Chen, G., Nelson, A., Fox-Kemper, B., 2018. Precession-band variance missing from East Asian monsoon runoff. Nat. Commun. 9, article 3364. https://doi.org/10.1038/s41467-018-05814-0

Duan, W., Cheng, H., Tan, M., Li, X., Edwards, R.L., 2019. Timing and structure of Termination II in north China constrained by a precisely dated stalagmite record. Earth Planet. Sci. Lett. 512, 1–7. https://doi.org/10.1016/j.epsl.2019.01.043

Duan, W., Wang, Xu, Tan, M., Cui, L., Wang, Xuefeng, Xiao, Z., 2022. Variable Phase Relationship Between Monsoon and Temperature in East Asia During Termination II Revealed by Oxygen and Clumped Isotopes of a Northern Chinese Stalagmite. Geophys. Res. Lett. 49, article e2022GL098296. https://doi.org/10.1029/2022GL098296

Esri (2023a). “Light Grey Canvas” [basemap] 1:66,623,747 (upper panel), 1:43,517 (lower panel). https://www.arcgis.com/home/item.html?id=979c6cc89af9449cbeb5342a439c6a76 (accessed 20/03/2023).

Esri (2023b). “World Hillshade” [basemap] 1:66,623,747 (upper panel), 1:43,517 (lower panel). https://www.arcgis.com/home/item.html?id=1b243539f4514b6ba35e7d995890db1d (accessed 20/03/2023).

Gorbarenko, S.A., Malakhova, G.Y., Artemova, A. V., Bosin, A.A., Yanchenko, E.A., Vasilenko, Y.P., 2019. Millennial scale cycles in the Bering Sea during penultimate and last glacials;

their similarities and differences. Quat. Int. 525, 151–158. https://doi.org/10.1016/j.quaint.2019.07.016

Grant, K.M., Rohling, E.J., Bronk Ramsey, C., Cheng, H., Edwards, R.L., Florindo, F., Heslop, D., Marra, F., Roberts, A.P., Tamisiea, M.E., Williams, F., 2014. Sea-level variability over five glacial cycles. Nat. Commun. 5, article 5076. https://doi.org/10.1038/ncomms6076

Hayashi, R., Takahara, H., Hayashida, A., Takemura, K., 2010. Millennial-scale vegetation changes during the last 40,000yr based on a pollen record from Lake Biwa, Japan. Quat. Res. 74, 91–99. https://doi.org/10.1016/j.yqres.2010.04.008

He, J., Jia, G., Li, L., Wang, P., 2017. Differential timing of C4 plant decline and grassland retreat during the penultimate deglaciation. Glob. Planet. Change 156, 26–33. https://doi.org/10.1016/j.gloplacha.2017.08.001

Holtvoeth, J., Whiteside, J.H., Engels, S., Freitas, F.S., Grice, K., Greenwood, P., Johnson, S., Kendall, I., Lengger, S.K., Lücke, A., Mayr, C., Naafs, B.D.A., Rohrssen, M., Sepúlveda, J., 2019. The paleolimnologist’s guide to compound-specific stable isotope analysis – An introduction to principles and applications of CSIA for Quaternary lake sediments. Quat. Sci. Rev. 207, 101–133. https://doi.org/10.1016/j.quascirev.2019.01.001

Jiang, X., Wang, Y., Kong, X., Wu, J., Shao, X., Xia, Z., Cheng, H., 2005. Abrupt climate change of East Asian Monsoon at 130 ka BP inferred from a high resolution stalagmite δ18O record. Chinese Sci. Bull. 50, 2765–2769. https://doi.org/10.1360/982004-819

Johnsen, S., Clausen, H.B., Dansgaard, W., Gundestrup, N.S., Hammer, C.U., Andersen, U., Andersen, K.K., Hvidberg, C.S., Steffensen, P., White, J., Jouzel, J., Fisher, D., 1997. The d180 record along the Greenland Ice Core Project deep ice core and the problem of possible Eemian climatic instability. J. Geophys. Res. 102, 26,397-26,410.

Kawamura, K., Parrenin, F., Lisiecki, L., Uemura, R., Vimeux, F., Severinghaus, J.P., Hutterli, M.A., Nakazawa, T., Aoki, S., Jouzel, J., Raymo, M.E., Matsumoto, K., Nakata, H., Motoyama, H., Fujita, S., Goto-Azuma, K., Fujii, Y., Watanabe, O., 2007. Northern Hemisphere forcing of climatic cycles in Antarctica over the past 360,000 years. Nature 448, 912–916. https://doi.org/10.1038/nature06015

Kelly, M.J., Edwards, R.L., Cheng, H., Yuan, D., Cai, Y., Zhang, M., Lin, Y., An, Z., 2006. High resolution characterization of the Asian Monsoon between 146,000 and 99,000 years B.P. from Dongge Cave, China and global correlation of events surrounding Termination II. Palaeogeogr. Palaeoclimatol. Palaeoecol. 236, 20–38. https://doi.org/10.1016/j.palaeo.2005.11.042

Kurita, N., Fujiyoshi, Y., Nakayama, T., Matsumi, Y., Kitagawa, H., 2015. East Asian Monsoon controls on the inter-annual variability in precipitation isotope ratio in Japan. Clim. Past 11, 339–353. https://doi.org/10.5194/cp-11-339-2015

Landais, A., Dreyfus, G., Capron, E., Jouzel, J., Masson-Delmotte, V., Roche, D.M., Prié, F., Caillon, N., Chappellaz, J., Leuenberger, M., Lourantou, A., Parrenin, F., Raynaud, D., Teste, G., 2013. Two-phase change in CO2, Antarctic temperature and global climate during Termination II. Nat. Geosci. 6, 1062–1065. https://doi.org/10.1038/ngeo1985

Laskar, J., Robutel, P., Joutel, F., Gastineau, M., Correia, A.C.M., Levrard, B., 2004. A long-term numerical solution for the insolation quantities of the Earth. Astron. Astrophys. 428, 261–285. https://doi.org/10.1051/0004-6361:20041335

Leipe, C., Nakagawa, T., Gotanda, K., Müller, S., Tarasov, P.E., 2015. Late Quaternary vegetation and climate dynamics at the northern limit of the East Asian summer monsoon and its regional and global-scale controls. Quat. Sci. Rev. 116, 57–71. https://doi.org/10.1016/j.quascirev.2015.03.012

Li, T.Y., Shen, C.C., Huang, L.J., Jiang, X.Y., Yang, X.L., Mii, H.S., Lee, S.Y., Lo, L., 2014. Stalagmite-inferred variability of the Asian summer monsoon during the penultimate glacial-interglacial period. Clim. Past 10, 1211–1219. https://doi.org/10.5194/cp-10-1211-2014

Lisiecki, L.E., Raymo, M.E., 2005. A Pliocene-Pleistocene stack of 57 globally distributed benthic δ 18O records. Paleoceanography 20, article PA1003. https://doi.org/10.1029/2004PA001071

Lisiecki, L.E., Stern, J. V, 2016. Regional and global benthic δ18O stacks for the last glacial cycle. Paleoceanography 31, 1368–1394. https://doi.org/10.1002/2016PA003002

Loulergue, L., Schilt, A., Spahni, R., Masson-Delmotte, V., Blunier, T., Lemieux, B., Barnola, J.M., Raynaud, D., Stocker, T.F., Chappellaz, J., 2008. Orbital and millennial-scale features of atmospheric CH4 over the past 800,000 years. Nature 453, 383–386. https://doi.org/10.1038/nature06950

Lupien, R.L., Russell, J.M., Pearson, E.J., Castañeda, I.S., Asrat, A., Foerster, V., Lamb, H.F., Roberts, H.M., Schäbitz, F., Trauth, M.H., Beck, C.C., Feibel, C.S., Cohen, A.S., 2022. Orbital controls on eastern African hydroclimate in the Pleistocene. Sci. Rep. 12, article 3170. https://doi.org/10.1038/s41598-022-06826-z

Marcott, S.A., Bauska, T.K., Buizert, C., Steig, E.J., Rosen, J.L., Cuffey, K.M., Fudge, T.J., Severinghaus, J.P., Ahn, J., Kalk, M.L., McConnell, J.R., Sowers, T., Taylor, K.C., White, J.W.C., Brook, E.J., 2014. Centennial-scale changes in the global carbon cycle during the last deglaciation. Nature 514, 616–619. https://doi.org/10.1038/nature13799

Masson-Delmotte, V., Stenni, B., Blunier, T., Cattani, O., Chappellaz, J., Cheng, H., Dreyfus, G., Edwards, R.L., Falourd, S., Govin, A., Kawamura, K., Johnsen, S.J., Jouzel, J., Landais, A., Lemieux-Dudon, B., Lourantou, A., Marshall, G., Minster, B., Mudelsee, M., Pol, K., Röthlisberger, R., Selmo, E., Waelbroeck, C., 2010. Abrupt change of antarctic moisture origin at the end of termination II. Proc. Natl. Acad. Sci. U. S. A. 107, 12091–12094. https://doi.org/10.1073/pnas.0914536107

McLean, D., Albert, P.G., Nakagawa, T., Suzuki, T., Staff, R.A., Yamada, K., Kitaba, I., Haraguchi, T., Kitagawa, J., Smith, V.C., 2018. Integrating the Holocene tephrostratigraphy for East Asia using a high-resolution cryptotephra study from Lake Suigetsu (SG14 core), central Japan. Quat. Sci. Rev. 183, 36–58. https://doi.org/10.1016/j.quascirev.2017.12.013

Meyers, P.A., Ishiwatari, R., 1993. Lacustrine organic geochemistry-an overview of indicators of organic matter sources and diagenesis in lake sediments. Org. Geochem. 20, 867–900. https://doi.org/10.1016/0146-6380(93)90100-P

Nakagawa, T., Gotanda, K., Haraguchi, T., Danhara, T., Yonenobu, H., Brauer, A., Yokoyama, Y., Tada, R., Takemura, K., Staff, R.A., Payne, R.L., Bronk Ramsey, C., Bryant, C.L., Brock, F., Schlolaut, G., Marshall, M.H., Tarasov, P.E., Lamb, H.F., 2012. SG06, a fully continuous and varved sediment core from Lake Suigetsu, Japan: Stratigraphy and potential for improving the radiocarbon calibration model and understanding of late Quaternary climate changes. Quat. Sci. Rev. 36, 164–176. https://doi.org/10.1016/j.quascirev.2010.12.013

Nakagawa, T., Tarasov, P., Staff, R., Bronk Ramsey, C., Marshall, M., Schlolaut, G., Bryant, C., Brauer, A., Lamb, H., Haraguchi, T., Gotanda, K., Kitaba, I., Kitagawa, H., van der Plicht, J., Yonenobu, H., Omori, T., Yokoyama, Y., Tada, R., Yasuda, Y., 2021. The spatio-temporal structure of the Lateglacial to early Holocene transition reconstructed from the pollen record of Lake Suigetsu and its precise correlation with other key global archives: Implications for palaeoclimatology and archaeology. Glob. Planet. Change 202, article 103493. https://doi.org/10.1016/j.gloplacha.2021.103493

Nakagawa, T., Tarasov, P.E., Kitagawa, H., Yasuda, Y., Gotanda, K., 2006. Seasonally specific responses of the East Asian monsoon to deglacial climate changes. Geology 34, 521–524. https://doi.org/10.1130/G21764.1

Nilsson-Kerr, K., Anand, P., Sexton, P.F., Leng, M.J., Misra, S., Clemens, S.C., Hammond, S.J., 2019. Role of Asian summer monsoon subsystems in the inter-hemispheric progression of deglaciation. Nat. Geosci. 12, 290–295. https://doi.org/10.1038/s41561-019-0319-5

Oba, T., Irino, T., Yamamoto, M., Murayama, M., Takamura, A., Aoki, K., 2006. Paleoceanographic change off central Japan since the last 144,000 years based on high-resolution oxygen and carbon isotope records. Glob. Planet. Change 53, 5–20. https://doi.org/10.1016/j.gloplacha.2006.05.002

Oppo, D.W., Sun, Y., 2005. Amplitude and timing of sea-surface temperature change in the northern South China Sea: Dynamic link to the East Asian monsoon. Geology 33, 785–788. https://doi.org/10.1130/G21867.1

Park, Jungjae, Park, Jinheum, Yi, S., Cheul Kim, J., Lee, E., Choi, J., 2019. Abrupt Holocene climate shifts in coastal East Asia, including the 8.2 ka, 4.2 ka, and 2.8 ka BP events, and societal responses on the Korean peninsula. Sci. Rep. 9, article 10806. https://doi.org/10.1038/s41598-019-47264-8

Rasmussen, S.O., Bigler, M., Blockley, S.P.., Blunier, T., Buchardt, S.L., Clausen, H.B., Cvijanovic, I., Dahl-Jensen, D., Johnsen, S.J., Fischer, H., Gkinis, V., Guillevic, M., Hoek, W.Z., Lowe, J., Pedro, J.B., Popp, T., Seierstad, I.K., Steffensen, J.-P., Svensson, A.M., Vallelonga, P., Vinther, B.M., Walker, M.J.., Wheatley, J.J., Winstrup, M., 2014. A stratigraphic framework for abrupt climatic changes during the Last Glacial period based on three synchronized Greenland ice-core records: Refining and extending the INTIMATE event stratigraphy. Quat. Sci. Rev. 106, 14–28. https://doi.org/10.1016/j.quascirev.2014.09.007

Rex, C.L., Staff, R.A., Sanderson, D.C.W., Cresswell, A.J., Marshall, M.H., Hyodo, M., Horiuchi, D., Tada, R., Nakagawa, T., 2022. Controls on luminescence signals in lake sediment cores: A study from Lake Suigetsu, Japan. Quat. Geochronol. 71, article 101319. https://doi.org/10.1016/j.quageo.2022.101319

Rex C.L., Staff, R.A., Leng, M.J., Toney, J.L., Pearson, E.J., Tyler, J.J., Swann, G.E.A., Lacey, J.H., Saito-Kato, M., Nakagawa, T., 2023 (preprint). Insights into deglacial East Asian Monsoon seasonality and inter-regional teleconnections from Lake Suigetsu, Japan. EarthArXiv. https://doi.org/10.31223/X56Q3N

Rex, C.L., Tyler, J.J., Nagaya, K., Staff, R.A., Leng, M.J., Yamada, K., Kitaba, I., Kitagawa, J., Kojima, H., Nakagawa, T., 2023 (preprint). The contemporary stable isotope hydrology of Lake Suigetsu and surrounding catchment (Japan) and its implications for sediment-derived palaeoclimate records. EarthArXiv. https://doi.org/10.31223/X53X2D

Rozanski, K., Araguás-Araguás, L., Gonfiantini, R., 2013. Isotopic Patterns in Modern Global Precipitation. Clim. Chang. Cont. Isot. Rec. https://doi.org/10.1029/gm078p0001

Sachse, D., Billault, I., Bowen, G.J., Chikaraishi, Y., Dawson, T.E., Feakins, S.J., Freeman, K.H., Magill, C.R., McInerney, F.A., van der Meer, M.T.J., Polissar, P., Robins, R.J., Sachs, J.P., Schmidt, H.-L., Sessions, A.L., White, J.W.C., West, J.B., Kahmen, A., 2012. Molecular Paleohydrology: Interpreting the Hydrogen-Isotopic Composition of Lipid Biomarkers from Photosynthesizing Organisms. Annu. Rev. Earth Planet. Sci. 40, 221–249. https://doi.org/10.1146/annurev-earth-042711-105535

Sachse, D., Radke, J., Gleixner, G., 2006. δD values of individual n-alkanes from terrestrial plants along a climatic gradient - Implications for the sedimentary biomarker record. Org. Geochem. 37, 469–483. https://doi.org/10.1016/j.orggeochem.2005.12.003

Schlolaut, G., Brauer, A., Marshall, M.H., Nakagawa, T., Staff, R.A., Bronk Ramsey, C., Lamb, H.F., Bryant, C.L., Naumann, R., Dulski, P., Brock, F., Yokoyama, Y., Tada, R., Haraguchi, T., 2014. Event layers in the Japanese Lake Suigetsu "SG06" sediment core: Description, interpretation and climatic implications. Quat. Sci. Rev. 83, 157–170. https://doi.org/10.1016/j.quascirev.2013.10.026

Schlolaut, G., Marshall, M.H., Brauer, A., Nakagawa, T., Lamb, H.F., Staff, R.A., Bronk Ramsey, C., Bryant, C.L., Brock, F., Kossler, A., Tarasov, P.E., Yokoyama, Y., Tada, R., Haraguchi, T., 2012. An automated method for varve interpolation and its application to the Late Glacial chronology from Lake Suigetsu, Japan. Quat. Geochronol. 13, 52–69. https://doi.org/10.1016/j.quageo.2012.07.005

Schlolaut, G., Staff, R.A., Brauer, A., Lamb, H.F., Marshall, M.H., Bronk Ramsey, C., Nakagawa, T., 2018. An extended and revised Lake Suigetsu varve chronology from ∼50 to ∼10 ka BP based on detailed sediment micro-facies analyses. Quat. Sci. Rev. 200, 351–366. https://doi.org/10.1016/j.quascirev.2018.09.021

Shigematsu, T., Tabushi, M., Nishikawa, Y., Muroga, T., Matsunaga, Y., 1961. Geochemical Study on Lakes Mikata. Bull. Inst. Chem. Res. Kyoto Univ. 39, 43–56.

Spratt, R.M., Lisiecki, L.E., 2016. A Late Pleistocene sea level stack. Clim. Past 12, 1079–1092. https://doi.org/10.5194/cp-12-1079-2016

Staff, R.A. (2011) Research on Radiocarbon Calibration Records, Focussing on New Measurements from Lake Suigetsu, Japan. University of Oxford.

Suzuki, Y., Tada, R., Yamada, K., Irino, T., Nagashima, K., Nakagawa, T., Omori, T., 2016. Mass accumulation rate of detrital materials in Lake Suigetsu as a potential proxy for heavy precipitation: a comparison of the observational precipitation and sedimentary record. Prog. Earth Planet. Sci. 3, article 5. https://doi.org/10.1186/s40645-016-0081-x

Thomas, E.K., Clemens, S.C., Prell, W.L., Herbert, T.D., Huang, Y., Liu, Z., Sinninghe Damsté, J.S., Sun, Y., Wen, X., 2014. Temperature and leaf wax δ^2H records demonstrate seasonal and regional controls on Asian monsoon proxies. Geology 42, 1075–1078. https://doi.org/10.1130/G36289.1

Tierney, J.E., Russell, J.M., Huang, Y., 2010. A molecular perspective on Late Quaternary climate and vegetation change in the Lake Tanganyika basin, East Africa. Quat. Sci. Rev. 29, 787–800. https://doi.org/10.1016/j.quascirev.2009.11.030

Tierney, J.E., Russell, J.M., Huang, Y., Sinninghe Damsté, J.S., Hopmans, E.C., Cohen, A.S., 2008. Northern Hemisphere controls on tropical southeast African climate during the past 60,000 years. Science. 322, 252–255. https://doi.org/10.1126/science.1160485

Tierney, J.E., Torfstein, A., Bhattacharya, T., 2022. Late Quaternary hydroclimate of the Levant : The leaf wax record from the Dead Sea. Quat. Sci. Rev. 289, article 107613. https://doi.org/10.1016/j.quascirev.2022.107613

van Bree, L.G.J., Peterse, F., van der Meer, M.T.J., Middelburg, J.J., Negash, A.M.D., De Crop, W., Cocquyt, C., Wieringa, J.J., Verschuren, D., Sinninghe Damsté, J.S., 2018. Seasonal variability in the abundance and stable carbon-isotopic composition of lipid biomarkers in suspended particulate matter from a stratified equatorial lake (Lake Chala, Kenya/Tanzania): Implications for the sedimentary record. Quat. Sci. Rev. 192, 208–224. https://doi.org/10.1016/j.quascirev.2018.05.023

WAIS Divide Project Members, Fudge, T.J., Steig, E.J., Markle, B.R., Schoenemann, S.W., Ding, Q., Taylor, K.C., McConnell, J.R., Brook, E.J., Sowers, T., White, J.W.C., Alley, R.B., Cheng, H., Clow, G.D., Cole-Dai, J., Conway, H., Cuffey, K.M., Edwards, J.S., Lawrence Edwards, R., Edwards, R., Fegyveresi, J.M., Ferris, D., Fitzpatrick, J.J., Johnson, J., Hargreaves, G., Lee, J.E., Maselli, O.J., Mason, W., McGwire, K.C., Mitchell, L.E., Mortensen, N., Neff, P., Orsi, A.J., Popp, T.J., Schauer, A.J., Severinghaus, J.P., Sigl, M., Spencer, M.K., Vaughn, B.H., Voigt, D.E., Waddington, E.D., Wang, X., Wong, G.J., 2013. Onset of deglacial warming in West Antarctica driven by local orbital forcing. Nature 500, 440–444. https://doi.org/10.1038/nature12376

Wang, Y., Cheng, H., Edwards, R.L., Kong, X., Shao, X., Chen, S., Wu, J., Jiang, X., Wang, X., An, Z., 2008. Millennial- and orbital-scale changes in the East Asian monsoon over the past 224,000 years. Nature 451, 1090–1093. https://doi.org/10.1038/nature06692

Wang, Y., Liu, X., Herzschuh, U., 2010. Asynchronous evolution of the Indian and East Asian Summer Monsoon indicated by Holocene moisture patterns in monsoonal central Asia. Earth-Science Rev. 103, 135–153. https://doi.org/10.1016/j.earscirev.2010.09.004

Wang, Y.J., Cheng, H., Edwards, R.L., An, Z.S., Wu, J.Y., Shen, C.C., Dorale, J.A., 2001. A high-resolution absolute-dated late pleistocene monsoon record from Hulu Cave, China. Science. 294, 2345–2348. https://doi.org/10.1126/science.1064618

Xu, H., Goldsmith, Y., Lan, J., Tan, L., Wang, X., Zhou, X., Cheng, J., Lang, Y., Liu, C., 2020. Juxtaposition of Western Pacific Subtropical High on Asian Summer Monsoon Shapes Subtropical East Asian Precipitation. Geophys. Res. Lett. 47, article e2019GL084705. https://doi.org/10.1029/2019GL084705

Xue, G., Cai, Y., Ma, L., Cheng, X., Cheng, H., Edwards, R.L., Li, D., Tan, L., 2019. A new speleothem record of the penultimate deglacial: Insights into spatial variability and centennial-scale instabilities of East Asian monsoon. Quat. Sci. Rev. 210, 113–124. https://doi.org/10.1016/j.quascirev.2019.02.023

Yuan, D., Cheng, H., Edwards, R.L., Dykoski, C.A., Kelly, M.J., Zhang, M., Qing, J., Lin, Y., Wang, Y., Wu, J., Dorale, J.A., An, Z., Cai, Y., 2004. Timing, Duration, and Transitions of the Last Interglacial Asian Monsoon. Science. 304, 575–578. https://doi.org/10.1126/science.1091220

Zhang, H., Brahim, Y.A., Li, H., Zhao, J., Kathayat, G., Tian, Y., Baker, J., Wang, J., Zhang, F., Ning, Y., Edwards, R.L., Cheng, H., 2019. The Asian Summer Monsoon: Teleconnections and Forcing Mechanisms—A Review from Chinese Speleothem δ18O Records. Quaternary 2, article 26. https://doi.org/10.3390/quat2030026

Zhang, H., Griffiths, M.L., Chiang, J.C.H., Kong, W., Wu, S., Atwood, A., Huang, J., Cheng, H., Ning, Y., Xie, S., 2018. East Asian hydroclimate modulated by the position of the westerlies during Termination I. Science. 362, 580–583. https://doi.org/10.1126/science.aat9393

Zhang, Y., Yu, J., Su, Y., Du, Y., Liu, Z., 2020. A comparison of n-alkane contents in sediments of five lakes from contrasting environments. Org. Geochem. 139, article 103943. https://doi.org/10.1016/j.orggeochem.2019.103943